Author/s:
Trajanovska, S;Ban, J;Huang, J;Gregorevic, P;Morsch, M;Allen, DG;Phillips, WD

Title:
Muscle specific kinase protects dystrophic mdx mouse muscles from eccentric contraction-induced loss of force-producing capacity

Date:
2019-09-01

Citation:
Trajanovska, S., Ban, J., Huang, J., Gregorevic, P., Morsch, M., Allen, D. G. & Phillips, W. D. (2019). Muscle specific kinase protects dystrophic mdx mouse muscles from eccentric contraction-induced loss of force-producing capacity. Journal of Physiology, 597 (18), pp.4831-4850. https://doi.org/10.1113/JP277839.

DOI: 10.1113/JP277839

Muscle Specific Kinase (MuSK) protects dystrophic *mdx* mouse muscles from eccentric contraction-induced loss of force-producing capacity

Trajanovska, S[1]*, Ban J[1]*, Huang, J[1], Gregorevic, P[2-5], Morsch, M[6], Allen, DG[1], Phillips, W.D.[1]

Running title: Muscle specific kinase protects dystrophic mouse muscle

[1] Physiology and Bosch Institute, University of Sydney, Sydney, NSW Australia
[2] Dept. of Physiology, The University of Melbourne, VIC, Australia
[3] Baker IDI Heart and Diabetes Institute, Melbourne, VIC 3004, Australia
[4] Dept. of Biochemistry and Molecular Biology, Monash University, VIC, Australia
[5] Dept. of Neurology, University of Washington School of Medicine, Seattle, WA, USA
[6] Department of Biomedical Sciences, Macquarie University, Sydney, NSW, Australia
*These authors contributed equally

Key words: neuromuscular junction, *mdx*, Duchenne muscular dystrophy, MuSK, rapsyn, muscle contraction

Corresponding author: William Phillips, Physiology, Anderson Stuart Bldg (F13)
University of Sydney, NSW 2006 Australia

Table of Contents category: Muscle

Key points summary:

- Adeno-associated viral vector was used to elevate the expression of MuSK and rapsyn in the tibialis anterior muscle of wild-type and dystrophic (*mdx*) mice.
- In *mdx* mice, enhanced expression of either MuSK or rapsyn ameliorated the acute loss of muscle force associated with strain injury.
- Increases in sarcolemmal immunolabelling for utrophin and beta-dystroglycan suggest a mechanism for the protective effect of MuSK in *mdx* muscles.
- MuSK also caused subtle changes to the structure and function of the neuromuscular junction, suggesting novel roles for MuSK in muscle physiology & pathophysiology.

Abstract:

Muscle specific kinase (MuSK) has a well-defined role in stabilizing the developing mammalian neuromuscular junction, but MuSK might also be protective in some neuromuscular diseases. In the dystrophin-deficient *mdx* mouse model of Duchenne muscular dystrophy, limb muscles are especially fragile. We injected the tibialis anterior muscle of 8-week old *mdx* and wild-type (C57BL10) mice with adeno-associated viral vectors encoding either MuSK or rapsyn (a cytoplasmic MuSK effector protein) fused to green fluorescent protein (MuSK-GFP and rapsyn-GFP respectively). Contralateral muscles injected with empty vector served as controls. One month later mice were anaesthetized with isoflurane and isometric force-producing capacity was recorded from the distal tendon. MuSK-GFP caused an unexpected decay in nerve-evoked tetanic force, both in wild-type and *mdx* muscles, without affecting contraction elicited by direct electrical stimulation of the muscle. Muscle fragility was probed by challenging muscles with a strain injury protocol consisting of a series of four strain-producing eccentric contractions *in vivo*. When applied to muscles of *mdx* mice, eccentric contraction produced an acute 27% reduction in directly-evoked muscle force output, affirming the susceptibility of *mdx* muscles to strain injury. *Mdx* muscles overexpressing MuSK-GFP or rapsyn-GFP exhibited significantly milder force deficits after the eccentric contraction challenge (15% and 14% respectively). The protective effect of MuSK-GFP in muscles of *mdx* mice was associated with increased immunolabelling for utrophin and β–dystroglycan in the sarcolemma. Elevating the expression of MuSK or rapsyn revealed several distinct synaptic and extra-synaptic effects, suggesting novel roles for MuSK signalling in muscle physiology and pathophysiology.

Sofie Trajanovska and Joanne Ban were joint first authors and equal contributors to this study. Sofie received her PhD in Molecular Physiology from Deakin University, Australia in 2009. She was later appointed a post-doctoral position at The University of Sydney investigating the effects of muscle fatigue and stretch-induced muscle damage. Currently she is working in the Preclinical Core Research Facility at the university, supporting translational research. Joanne received her Bachelor of Biomedical Sciences (Hons) from the University Putra Malaysia in 2013 and moved to Sydney to undertake a PhD in Medicine at the University of Sydney, graduating in 2018. Her thesis work focused on understanding the role of neuromuscular junction signalling proteins in healthy muscle and in the *mdx* mouse model of Duchenne Muscular Dystrophy.

Introduction

Muscle specific kinase (MuSK; a transmembrane tyrosine kinase) is known for its essential role in formation of the neuromuscular junction (NMJ; (DeChiara *et al.*, 1996)), and remains highly concentrated at motor endplates of mature fast-type muscle fibres (Valenzuela *et al.*, 1995). The kinase activity of MuSK is strongly increased by neural agrin, a proteoglycan ligand produced by the motor nerve, which binds the low-density lipoprotein receptor related protein 4 (LRP4) to form an agrin-LRP4-MuSK protein complex (Kim *et al.*, 2008; Zhang *et al.*, 2008). A local phosphorylation cascade then recruits the cytoplasmic effector protein, rapsyn. Rapsyn, in turn, helps stabilize postsynaptic acetylcholine receptors (AChRs; (Borges *et al.*, 2008; Brockhausen *et al.*, 2008; Luo *et al.*, 2008)). MuSK activation also slows the proteasomal degradation of rapsyn, thereby raising the concentration of rapsyn in the cytoplasm (Brockhausen *et al.*, 2008; Luo *et al.*, 2008). Another cytoplasmic protein, called DOK7, increases the kinase activity of MuSK by binding and stabilizing MuSK dimers (Bergamin *et al.*, 2010). Recently, recombinant adeno-associated viral vectors (AAV vectors) have been used to elevate muscle expression of either MuSK or DOK7 in transgenic mouse models of Emery-Dreifuss muscular dystrophy or amyotrophic lateral sclerosis. This was associated with improved retention of neuromuscular connections and muscle strength (Perez-Garcia & Burden, 2012; Arimura *et al.*, 2014; Miyoshi *et al.*, 2017). These studies raise the question of whether MuSK might be beneficial in other neuromuscular diseases.

Duchenne muscular dystrophy (DMD) is a fatal X-linked genetic disease caused by a complete loss of the sarcolemma-associated protein, dystrophin (Yiu & Kornberg, 2015). Dystrophin is a key component of the dystrophin-associated protein (DAP) complex that helps couple sarcomeres, through the sarcolemma, to the extracellular matrix. The absence of dystrophin de-stabilizes other core proteins of the DAP complex, including dystroglycan, predisposing muscle fibres to multiple cycles of fibre necrosis and regeneration. This leads to chronic inflammatory changes, fibrosis and premature death, often due to respiratory or cardiac failure (Yiu & Kornberg, 2015 ; Ryder *et al.*, 2017). *The mdx* mouse, which is dystrophin-null (due to a point mutation in exon 23) is the most extensively studied animal model of DMD (reviewed by (Grounds *et al.*, 2008; Manning & O'Malley, 2015)). The fragility of *mdx* muscles is often demonstrated by measuring the acute drop in maximum tetanic force that occurs when the muscle is challenged with a series of eccentric contractions (EC). The forced lengthening during maximum tetanic activation that occurs during EC

subjects the muscle to strain. In *mdx* mice, EC challenge can cause a more severe reduction in force-producing capacity and greater structural damage than if an identical EC series were applied to wild-type muscles (Brussee *et al.*, 1997; Dellorusso *et al.*, 2001; Whitehead *et al.*, 2006). In *mdx* muscles, the loss of dystrophin and DAPs is thought to make the fibres fragile and prone to elevated intracellular calcium and reactive oxygen species, membrane damage, impaired excitation-contraction coupling, sarcomere damage, and necrosis with regeneration of branched fibres that are more prone to further injury (Gumerson & Michele, 2011; Johnson *et al.*, 2013; Faber *et al.*, 2014; Allen *et al.*, 2016; Kiriaev *et al.*, 2018).

The degree of involvement of the NMJ in the pathophysiology of DMD and the *mdx* mouse remains uncertain (Lyons & Slater, 1991; Carlson & Roshek, 2001; van der Pijl *et al.*, 2016). Recently, Lovering and colleagues reported that MuSK mRNA and protein levels were reduced in quadriceps muscles of *mdx* mice, compared to wild-type mice (Pratt *et al.*, 2013; Pratt *et al.*, 2015a). Using immunofluorescence and confocal imaging they also reported quantitative differences in the structure of NMJs in quadriceps muscles of *mdx* mice, compared to wild-type mice. Firstly, they confirmed earlier reports that the postsynaptic acetylcholine receptor (AChR) clusters are more fragmented in *mdx* mice. Secondly they reported that, in *mdx* mice, the postsynaptic AChRs were less-well covered by synaptophysin-labelled nerve terminals, and neurofilament labelling revealed excess terminal branching with more axon terminal discontinuities (Pratt *et al.*, 2015b). Thirdly, they found that when *mdx* muscles were challenged with a series of ECs, endplate AChR clusters became even more fragmented and there was a reduction in the magnitude of the compound muscle action potential. These findings suggested that injury to the NMJ might contribute to the acute drop in strength that occurs when *mdx* muscles are challenged with a series of ECs (Pratt *et al.*, 2013; Pratt *et al.*, 2015a). Others have presented evidence that EC causes an acute drop in muscle fibre excitability, and that this contributes to the loss of force (Call *et al.*, 2013; Pratt *et al.*, 2013; Roy *et al.*, 2016). Here we have used an AAV vector to elevate the expression of MuSK in the tibialis anterior (TA) muscles of wild-type and *mdx* mice. We report that extra MuSK partially protected *mdx* muscles from the acute EC-induced loss of muscle strength. This protective effect of MuSK-GFP was evident even when the muscle was stimulated directly: bypassing the NMJ. Elevating rapsyn expression provided a similar degree of protection. These results suggest that MuSK and rapsyn can act downstream of

neuromuscular transmission to protect dystrophin-deficient muscles from acute stretch-induced injury.

Methods

Animals

All mouse experiments were conducted with the approval of the University of Sydney Animal Ethics Committee in compliance with the NSW Animal Research Act 1985 and the Australian Code of Practice for the Care and Use of Animals for Scientific Purposes 8th Edition NHMRC 2013. Eight-week old male wild-type (C57BL10ScSn; MGI Cat# 3581842, RRID:MGI:3581842) and *mdx* (C57BL/10ScSn-Dmd^{mdx}) mice were purchased from the Animal Resources Centre (WA, Australia) and housed in the Bosch Rodent Facility at the University of Sydney under a 12-hour light/dark cycle (dark at night). Mice had *ad libitum* access to food and water. A total of 38 mice were used in this study. They were group housed in individually ventilated cages (2-4 per cage). The authors understand the ethical principles under which the journal operates and confirm that the work described in this paper complies with the journal's animal ethics checklist.

AAV vector injections

Construction of cytomegalovirus promoter-driven MuSK-GFP and rapsyn-GFP expression cassettes, their packaging into AAV serotype 6 capsids and the intramuscular injection of the AAV preparations were detailed previously (Blankinship *et al.*, 2004; Ghazanfari *et al.*, 2015). Animal anaesthesia was induced with 4% isoflurane in oxygen then maintained at 1.5-2% via a rodent face-mask, adjusted to ensure full suppression of the foot withdrawal reflex (toe pinch) and steady breathing. The TA muscle was surgically exposed and a Hamilton syringe with a 32-gauge needle was used to inject 20µl of 0.9% sterile NaCl containing 2x 10^9 AAV vector genomes into the muscle belly. Intramuscular injection of AAV serotype 6 vectors at this dosage was previously found to ensure efficient expression across the injected muscle (Blankinship *et al.*, 2004; Ghazanfari *et al.*, 2015). The contralateral TA was injected with empty AAV vector (no transgene) to serve as a control. The wound was closed with suture and buprenorphine was administered for analgesia (0.03mg/kg, subcutaneously; Reckitt Benckiser, Australia). Mice were monitored for full recovery from anaesthesia and were subsequently inspected for wound healing and general health status twice weekly. Fig

1A shows the experimental timeline. Our primary purpose in this study was to test the influence of elevated MuSK/rapsyn upon the properties of intact muscle fibres. For this reason AAV injections were made at 8-weeks postnatal, after the period of florid muscle fibre necrosis/regeneration that occurs in *mdx* mice (McGeachie *et al.*, 1993; Duddy *et al.*, 2015). Mice were anaesthetized (without recovery) for contraction analysis and histology 34 (5) days after the AAV injections: to allow sufficient time for expression of the transgene throughout the muscle (Fig 1), and because force drop after EC challenge is readily demonstrated in *mdx* muscles at 2-3-months of age (Dellorusso *et al.*, 2001). Unilateral intramuscular injection of AAV-MuSK, paired with contralateral control muscles was chosen (rather than systemic AAV delivery) so as to reduce the number of animals required.

Contraction force experiments

Mice were anaesthetised as above, but without recovery. The mouse was placed on a heating pad regulated by a rectal thermosensor (37°C). The depth of isoflurane anaesthesia was monitored and maintained throughout the experiment by regularly testing the toe-pinch foot withdrawal reflex and monitoring respiratory rate. The following protocol was performed on each TA muscle (transgene-expressing and contralateral empty-vector control). The TA muscle was surgically exposed and a silk thread was tied around the distal tendon. The other end of the thread was fastened to a hook on the lever arm of a dual-mode servomotor/force transducer (Aurora Scientific). The leg was anchored using a clamp along the tibia in order to limit movement artefact during recordings. Data were captured on a personal computer using AxoScope software (Axon Instruments). Contraction force was recorded in response to both nerve-stimulation and direct muscle stimulation. For nerve stimulation, a pair of custom platinum wire electrodes was placed on the peroneal nerve to deliver 0.2 msec supramaximal square wave pulses in trains of 400 msec duration. A second pair of electrodes was placed on the surface of the muscle, perpendicular to the long axis of the fibres, to deliver trains of 0.5 msec supramaximal square wave pulses. The muscle and nerve were kept moist by direct application of warm HEPES-buffered Tyrode's solution (35°C). Each individual muscle was adjusted to optimal muscle length (L_o) for maximum isometric tetanic force. The stimulation frequency was varied so as to determine the maximum tetanic force (typically 150Hz). Specific force (mN/mm^2) was determined by normalizing maximum tetanic force for muscle cross-sectional area [(force (N) x length (mm) x density (1.06 $mg.mm^{-3}$))/muscle mass (mg)]. Maximum tetanic force was defined as the highest isometric force generated at any point in

the tetanic stimulation. The decline in nerve-evoked force observed in muscles expressing MuSK-GFP was measured as the difference between maximum force (near the beginning of the 400-msec tetanus) and the force remaining at the end of the tetanus (Fig 2Aa, 2D & E).

After determining maximum isometric force, the muscle was subjected to a series of ECs. To generate ECs the muscle was stimulated directly with a supramaximal stimulus (6-10V). Half way through the maximal 400msec tetanus the servomotor imposed a 1.25-fold lengthening beyond the optimal fibre length (L_f) with a stretching velocity of 2 × L_f/sec, as shown in Figure 3A. Each muscle was subjected to four such ECs, each separated by a 20 sec rest. Maximum isometric force was recorded before (initial force), and at 10 min intervals after this stretch protocol to assess the muscle injury/recovery, until the force reached a stable plateau value (typically 50 min after the EC protocol).

The final maximum isometric tension determination was used to calculate the force remaining, expressed as a percentage of the initial maximum isometric force (immediately before the ECs). At the conclusion of force recordings the mouse was euthanized by intraperitoneal injection of pentobarbitone (30mg; Cenvet, Australia) and muscles were collected for immunoblotting and immunofluorescence. A 'recovery score' (Willmann *et al.*, 2012) was used to assess the ability of AAV-MuSK-GFP to prevent EC-induced loss of initial muscle force. It was calculated as follows:

$$\text{Recovery score (\%)} = \frac{[\text{MuSK treated } mdx] - [\text{empty vector } mdx]}{[\text{empty vector wt}] - [\text{empty vector } mdx]} \times 100$$

Where the square brackets represent the % of the initial, directly-evoked, force remaining after the EC challenge for the indicated muscle groups.

Antibodies and immunoblotting for dystrophin-associated proteins

Muscles were snap frozen in liquid nitrogen and stored at -80°C. Whole frozen muscles were pulverized under liquid nitrogen with a mortar and pestle then solubilized in 4 volumes of lysate buffer at 100°C for 2 minutes (1% SDS, 5mM EGTA, 1mM benzamidine, 10µM leupeptin and 0.2mM PMSF). Muscle extracts were centrifuged at 21,000 x g for 3 minutes and the supernatant was transferred to a clean centrifuge tube and stored at -80°C. Protein concentration was determined by Direct Detect® spectrophotometry (Merck Millipore, Vic, Australia). SDS-PAGE followed by standard immunoblotting was used to validate the antibodies. Two different antibodies were used to detect β-dystroglycan. To compare levels

of β-dystroglycan in homogenates we used the mouse monoclonal IgG MANDAG2(7D11) (Pereboev *et al.*, 2001), obtained from the Developmental Studies Hybridoma Bank (DSHB, Cat# MANDAG2(7D11), RRID:AB_2618140). On standard immunoblots of wild-type muscle extract, MANDAG2(7D11) strongly labelled a band approximating the established molecular mass of β-dystroglycan (~43kD; Fig 7, to the right of panel C;(Barresi & Campbell, 2006)). An additional weak band at approximately 30kD is similar to the predicted molecular mass of β-dystroglycan polypeptide without post-translational modifications (26kD). For immunofluorescence (detailed below) we used affinity purified rabbit polyclonal β-dystroglycan antibody (1:500, a kind gift from Dr Vann Bennett) which was characterized previously (Ayalon *et al.*, 2008). Rabbit anti-α1-syntrophin (1:2000, Thermo Fisher Scientific, Cat# pa1-25013, RRID:AB_2191932) was also used for immunofluorescence. On western blot this antibody yielded a band in the expected molecular weight range: 54-58kD ((Adams *et al.*, 2000); Fig 7 blot next to panel F). For quantifying β-dystroglycan, protein bands were separated and probed with antibodies using an automated capillary electrophoresis based system (Wes™ system; Bio-techne, Minneapolis, MN). On this system, β-dystroglycan (probed with MANDAG2(7D11)) ran at an estimated molecular mass of 48kD (Fig 7I). A commercial rabbit polyclonal anti-β-dystroglycan (Abcam, Cat# ab43125, RRID:AB_955822) detected precisely the same band at 48kD (data not shown). For each muscle sample the area under the 48kD intensity peak was divided by the area of the GAPDH loading control peak for the same sample, run in a parallel capillary (Abcam, Cat# ab9485, RRID:AB_307275). This corrected value was then normalized to the mean for the wild-type samples. The muscle samples (n=4 *mdx* mice) were run twice (technical replicates) and the resulting mean values for each muscle sample are presented in Fig 7J. The Wes™ system was also used to probe for utrophin. Each capillary was loaded with 3µg of muscle extract and was probed with 10µl of a 1:50 dilution of monoclonal antibody MANCHO-3 (DSHB Cat# MANCHO3(8A4), RRID:AB_2618137). Compass for SW software (version 4.0.0, ©Protein Simple) was used to scan the capillaries and detect peaks of antibody binding. Results are presented as virtual Western blots.

Immunofluorescence labelling and microscopy

For double labelling of AChR and synaptophysin (Fig 5A-F), muscles were dissected, weighed and fixed for 2 h in 4% paraformaldehyde. After rinsing in PBS and soaking overnight at 4°C in 20% sucrose/PBS, muscles were embedded in Tissue-Tek O.C.T.

compound (ProSciTech Australia) and rapidly frozen in isopentane (pre-chilled with liquid nitrogen). Longitudinal cryosections (20μm) were washed in PBS, immersed in 0.1 M glycine/PBS for 30min and permeabilised for 7 min in chilled methanol. After washing in PBS, sections were incubated for 1 h at room temperature in blocking solution (0.2% Triton X-100, 2% bovine serum albumin/PBS) and were incubated overnight at 4°C with rabbit anti-synaptophysin as a nerve terminal marker (1:200; Thermo Fisher Scientific, Cat# 18-0130, RRID:AB_10836766). Slides were then washed 3 times in PBS, and incubated for 1h at room temperature in blocking solution containing a mixture of Cy3-conjugated affinity-purified donkey anti-rabbit IgG (1:200; Jackson ImmunoResearch Labs, Cat# 711-165-152, RRID:AB_2307443) plus Alexa647-α-bungarotoxin to label postsynaptic AChRs (Alexa647-BGT; 1:200; Thermo Fisher Scientific, Cat# B35450). Coverslips were mounted with polyvinyl alcohol mounting medium (Sigma-Aldrich, MO). Sections were imaged on a Zeiss LSM 510 Meta confocal microscope using a ×40 1.2 NA air objective at 15% laser power (all channels). The pinhole diameter was set to 1.0 Airy unit for the Alexa647-α-BGT channel and then adjusted to ensure the same optical slice thickness for the other channels. Imaging parameters (gain and offset level) were optimized for each individual NMJ so as to maximize the visual information used to discern the area of synaptic specialization (Cheng *et al.*, 2013; Tse *et al.*, 2014). Enface Z-projection images of motor endplates (7 - 45 per muscle), were randomly sampled and ImageJ software was used to assess the area of postsynaptic AChRs, MuSK-GFP/rapsyn-GFP and presynaptic synaptophysin, using methods described previously (Tse *et al.*, 2014). The average endplate areas for each muscle are plotted as symbols in Fig 5G-J.

In order to compare the intensity of immunofluorescence in the sarcolemma between samples, transverse muscle cryosections were all processed as a batch and were imaged during the same confocal microscope session using fixed confocal settings. AChR were labelled with Alexa555-α-bungarotoxin (1:200, Thermo Fisher Scientific, Cat# B35451). ImageJ was used to draw a line around each crescent-shaped endplate in transverse confocal images and quantify the AChR intensity (Fig 5K-L;(Cheng *et al.*, 2013; Tse *et al.*, 2014)). To compare the subcellular distributions of MuSK (Fig 6) sections were double labelled with Alexa555-α-bungarotoxin and affinity purified sheep anti-MuSK, as described and characterized previously (Cole *et al.*, 2010). After washing three times, sections were incubated in Cy5-donkey anti-goat IgG, which recognises the, closely-related, sheep IgG

(1:50 Jackson ImmunoResearch Labs, Cat# 713-175-147, RRID:AB_2340730). To compare the sarcolemmal density of DAPs (Fig 7) sections were labelled with rabbit anti-α-syntrophin (1:2000, Thermo Fisher Scientific, Cat# pa1-25013, RRID:AB_2191932), or rabbit polyclonal β-dystroglycan antibody (1:500; a kind gift from Dr Vann Bennett). Primary antibody binding was then detected with Alexa647-donkey anti-rabbit IgG (1:200; Jackson ImmunoResearch Labs, Cat# 711-605-152, RRID:AB_2492288). Sections were imaged on a Leica DM-IRE2 inverted confocal microscope equipped with a Leica TCS SP2 system (Leica Microsystems, Sydney, Australia). Utrophin was immunolabeled with a mouse monoclonal antibody DRP3/20C5 (NCL-DRP2, 1:10, Leica Biosystems, Germany). The specificity of this antibody for labelling utrophin by immunofluorescence was previously demonstrated by comparing muscles from wild-type and utrophin$^{-/-}$ mice (Deconinck *et al.*, 1997). Utrophin-labelled sections were imaged on a Zeiss 510META confocal microscope (Carl Zeiss, Jena, Germany) with a 40x air objective and 561nm laser line. To avoid biased sampling, every field from each section was examined by moving from left to right and back in a systematic manner until images of a minimum of 20 endplates were collected from each muscle (Ghazanfari *et al.*, 2014). To compare the relative intensities of sarcolemmal fluorescence, ImageJ was used to draw a straight line perpendicularly through the extra-synaptic sarcolemma and/or the endplate. The 'Plot profile' tool was used to reveal peaks of membrane fluorescence intensity that occurred as the line passed through the sarcolemma. Peak heights for fluorescence intensity were averaged after correcting for background fluorescence. Control sections (no primary antibody) confirmed that the peaks of immunofluorescence were due to binding of the primary antibody.

Transverse cryosections of unfixed muscles were also used to assess muscle pathology. Sections were dried onto slides and muscle membranes were labelled overnight at 4°C with 1:300 Alexa555-conjugated wheat-germ agglutinin (Thermo Fisher Scientific, Cat# W32464) in 1% BSA/PBS. Nuclei were then counterstained for 1h with 1:1250 DAPI (Thermofischer). Digital montage images of whole muscle cross sections were collected by Widefield Axioscan Z1 virtual microscopy (Zeiss, Germany). A grid was overlaid on the virtual whole muscle cross section image and every fifth square in the grid was scored for the percentage of muscle fibres with centralised nuclei and to measure the Feret's minimum diameter of fibres. This was repeated until a minimum number of 250 muscle fibres were quantitated. For this particular analysis the observer was blinded to the treatment group of the muscle images.

Statistical analysis

Data are presented in the text as mean (SD) and were assumed to follow a normal distribution based upon visual inspection of the data plots. An exception was the very low density of endogenous MuSK in the extrasynaptic sarcolemma of fibres, resulting in a highly skewed distribution (Fig 6C). For every statistical test the sample size, *n*, was the number of muscles/mice. Histograms display the means and 95% confidence intervals, with superimposed symbols showing results for each individual muscle. Statistical analyses were performed using GraphPad Prism 7.0b for Mac OS X (San Diego CA). One-way ANOVA followed by Tukey's post-test was used to assess the relative effects of MuSK-GFP and rapsyn-GFP compared to control muscles (injected with empty-vector). Unpaired two-tailed Student's t-tests were used for comparison of two groups. Welch's correction was applied when the variances were found to be not equal. The significance level was set at $p<0.05$.

Results

Effects of MuSK-GFP upon nerve-evoked muscle force

Direct electrical stimulation of wild-type control muscles (C57BL10 mice injected with empty AAV vector) elicited the expected steady contraction and a maximum isometric force of 204 (31) mN/mm^2 (n=16 muscles). Contralateral muscles, expressing either MuSK-GFP or rapsyn-GFP, produced very similar steady force values when directly stimulated (Fig 2B). However when stimulated via the nerve, muscles expressing MuSK-GFP revealed a distinct 32 (6)% decay of force during the 400msec tetanus (Figs 2Aa dashed trace, 2D stippled bar). Direct stimulation of *mdx* empty-vector control muscles elicited a steady maximum force of 172 (23) mN/mm^2 (n=18). Direct stimulation of contralateral muscles, expressing MuSK-GFP or rapsyn-GFP produced very similar force values. As with the wild-type muscles, *mdx* muscles expressing MuSK-GFP revealed a distinct decay in nerve-evoked force, compared to empty-vector control muscles (Fig 2E). In the case of *mdx* muscles, at least, the decay in force was associated with a reduction in maximum nerve-evoked force (Fig 2C). In summary, overexpression of MuSK-GFP (but not rapsyn-GFP) caused an unanticipated decay in nerve-evoked muscle force production, in both wild-type and *mdx* mice.

MuSK-GFP and rapsyn-GFP protect mdx muscles from EC-induced force loss

The key question of the present study was to assess the impact of MuSK upon the fragility of *mdx* muscle fibres. To this end, muscles were challenged for resistance to strain injury with a series of four ECs. Based on the above findings (Fig 2) muscles were stimulated directly (bypassing the NMJ), to ensure that all muscle fibres were activated throughout the ECs. Figure 3A illustrates a single EC: a controlled 1.25 fold lengthening superimposed upon the maximum tetanic activation, with the associated increase in tension. Maximum isometric force was measured (both directly-evoked and nerve-evoked) before and after a series of four such ECs (see *Methods*). Wild-type muscles were resistant to this EC challenge (Fig 3B), retaining 95 (6)% of their initial force in response to a direct stimulation, and 92 (4)% of their initial nerve-evoked force (n=6; Fig 3B open bars). Wild-type muscles expressing MuSK-GFP or rapsyn-GFP were similarly resistant to the EC challenge (Fig 3B, stippled and hatched bars respectively). After an identical EC challenge, *mdx* empty-vector control muscles retained only 73 (6)% of their initial, directly-evoked force, and 69 (7)% of their nerve-evoked force (n=11; Fig 3C, open bars). Remarkably, *mdx* muscles expressing MuSK-GFP retained significantly more of their initial, directly-evoked force and nerve-evoked force after the EC challenge (85 (3)% and 85 (5)%; n=6 and 5 respectively), compared to *mdx* control muscles. This represents a 'recovery score' (Willmann *et al.*, 2012) for force retention of 54% relative to the, EC-resistant, wild-type control muscles (See *Methods*). Rapsyn-GFP also improved retention of directly-evoked and nerve-evoked force by *mdx* muscles (86 (6)% and 85 (5)%, n=5), compared to *mdx* empty-vector muscles (Fig 3C). In summary, the EC challenge caused an acute reduction in the maximum force capacity of *mdx* muscles as predicted, but *mdx* muscles expressing either MuSK-GFP or rapsyn-GFP were more resistant to this EC-induced injury.

Muscle pathology was not reversed by MuSK-GFP

In *mdx* mice the percentage of muscle fibres with centralised nuclei (regenerated fibres) rises abruptly from about 24 days postnatal reaching a plateau by about 8 weeks of age (Carnwath & Shotton, 1987; McGeachie *et al.*, 1993). Injecting AAV-MuSK-GFP into *mdx* muscles at 8-weeks of age did not reverse the high percentage of fibres with centralized nuclei, nor did it change the distribution of *mdx* muscle fibre diameters (Fig 4).

MuSK-GFP reduces motor endplate size in mdx muscles

Motor endplates from wild-type empty-vector control muscles consisted of the classic 'pretzel-like' arrangement with 3.2 (1.0) large postsynaptic AChR plaques (Fig 5A), whereas *mdx* endplates were more fragmented, consisting of groupings of 7.2 (1.3) smaller AChR clusters (Fig 5D; (Lyons & Slater, 1991; Pratt *et al.*, 2013; Ghazanfari *et al.*, 2015; van der Pijl *et al.*, 2016)). The total AChR-rich area per endplate was greater for *mdx* control muscles than for wild-type control muscles (400 (32) μm^2 versus 329 (53) μm^2; p=0009, n=11; unpaired t-test), This is consistent with previous findings for untreated *mdx* versus wild-type muscles (Lyons & Slater, 1991; Pratt *et al.*, 2013). The area of synaptophysin-labelled nerve terminals was also larger at *mdx* control endplates compared to wild-type control endplates (316 (34) μm^2 versus 257 (68) μm^2); p=0.02, n=11, t-test with Welch's correction). While the *mdx* endplate specializations were larger, the proportion of the AChR rich endplate area covered by nerve terminal was similar for the two genotypes (77% and 75% respectively).

Wild-type motor endplates expressing MuSK-GFP or rapsyn-GFP were similar in gross appearance to untreated and empty-vector control endplates (Fig 5A-C; (Lyons & Slater, 1991; Pratt *et al.*, 2013; Ghazanfari *et al.*, 2015; van der Pijl *et al.*, 2016)). MuSK-GFP did not alter the average area of postsynaptic AChR or presynaptic synaptophysin per wild-type endplate (Fig 5G&I). MuSK-GFP had no significant effect on the density of AChR in the postsynaptic membrane of wild-type (C57BL10) endplates (Fig 5K), consistent with our previous findings in wild-type C57BL6J mice (Ghazanfari *et al.*, 2015). In contrast, m*dx* muscles that expressed MuSK-GFP displayed reductions in NMJ size and AChR labelling. The mean area of AChR per endplate was reduced by 29% compared to *mdx* empty-vector control muscles (Fig 5H). There was a proportionate (28%) reduction in the area of nerve terminal synaptophysin labelling (Fig 5J). Muscles of *mdx* mice expressing rapsyn-GFP revealed a modest, 14%, reduction in the area of AChR per endplate (Fig 5H, hatched bar). In *mdx* muscles, MuSK-GFP also caused a reduction in the intensity of endplate AChR labelling (Fig 5L). These *mdx*-specific effects of MuSK-GFP upon the NMJ are intriguing, but they cannot explain the reduction in nerve-evoked force that we recorded in wild-type muscles expressing MuSK-GFP (Fig 2B&D and see *Discussion*).

AAV-MuSK vector expands MuSK expression into the sarcolemma

We used an antibody against MuSK to assess the subcellular distribution of MuSK within *mdx* muscle fibres. In wild-type fast-twitch muscle fibres MuSK is expressed mainly at the

endplate (Valenzuela *et al.*, 1995). In our analysis the average intensity of MuSK immunofluorescence at the endplate of *mdx* control muscles was 73 (16)% of the wild-type control value. In *mdx* muscles injected with AAV-MuSK-GFP this rose to 160 (65)% of the wild-type MuSK value. More obvious was the appearance of MuSK in the extrasynaptic sarcolemma of muscles injected with AAV-MuSK-GFP (Fig 6A & B). In wild-type and *mdx* control muscles only a few percent of muscle fibres displayed strong (endogenous) MuSK immunolabelling in their extrasynaptic sarcolemma (Fig 6C open bars). After injection of AAV-MuSK-GFP, the majority of muscle fibres displayed moderate to strong MuSK immunofluorescence in their sarcolemma (Fig 6C stippled bars). Thus, injection of AAV-MuSK-GFP led to MuSK being expressed throughout the sarcolemma of TA muscle fibres, a distribution of MuSK characteristic of the soleus muscle (Punga *et al.*, 2011).

Elevated MuSK increases utrophin and β-dystroglycan labelling in the mdx sarcolemma

Finally we examined the sarcolemmal density of β-dystroglycan, because dystroglycan is one of the DAPs that is expressed at reduced levels in *mdx* muscle fibres (Ohlendieck & Campbell, 1991; Johnson *et al.*, 2013), and because targeted knock-down of dystroglycan made (non-dystrophic) muscle fibres prone to EC-induced loss of strength (Rader *et al.*, 2016). The average intensity of β-dystroglycan immunofluorescence in the extrasynaptic sarcolemma of our *mdx* control muscles was 60 (12) % of the wild-type muscle level. Importantly, this rose to 90 (16) % in contralateral muscles injected with AAV-MuSK-GFP ($p=0.0058$ unpaired t-test; Fig 7A-C & G). In contrast there was no change in the intensity of sarcolemmal immunofluorescence for α-syntrophin, a cytoplasmic DAP ($p=0.47$; Fig 7D-F & H). Whole muscle homogenates probed with anti-β-dystroglycan antibody revealed an increase in total β-dystroglycan protein (Fig 7I & J). Since utrophin can protect β-dystroglycan from rapid ubiquitin-mediated degradation (Choa *et al.*, 2018) and stabilize the sarcolemma, we next used immunofluorescence to visualize utrophin in the sarcolemma. Consistent with previous studies, dim utrophin immunofluorescence could be seen in the extrasynaptic sarcolemma of *mdx* control (empty vector) muscles but not in wild-type muscles (Fig 8B & A respectively). Interestingly, utrophin immunofluorescence was about 3-fold more intense in the sarcolemma of *mdx* muscles after injection of AAV-MuSK, compared to contralateral empty-vector control muscles (Fig 8B-D). The density of MuSK-GFP in the sarcolemma varied considerably from fibre to fibre within a given muscle (Fig 6C), possibly due to random variability in the uptake and expression of AAV vector by

individual fibres. Importantly, the intensity of utrophin immunofluorescence in the sarcolemma of a given fibre was positively correlated with the intensity of MuSK-GFP fluorescence in the same patch of membrane, suggesting a direct relationship between the membrane densities of MuSK and utrophin (Fig 8E). The Wes™ capillary electrophoresis system and anti-utrophin antibody was used to probe whole muscle extracts from *mdx* mice. Three of four *mdx* mouse muscles that had been injected with AAV-MuSK displayed a band approximating utrophin's predicted molecular mass of 392kDa (Fig 8F, *mdx* + MuSK). In contrast, scans of the four contralateral control muscles (*mdx* empty) and three untreated wild-type muscles revealed no detectable utrophin band (Fig 8F). Presumably the sensitivity of the assay was insufficient to detect the amount of utrophin present in the latter extracts. Together, the results suggest that elevating MuSK expression in the extra-synaptic sarcolemma of *mdx* muscle fibres can help restore utrophin and dystroglycan to the sarcolemma and this may help protect muscles from EC-induced injury.

Discussion

Recent studies have suggested that enhanced expression of MuSK or DOK7 might be beneficial in mouse models of neuromuscular disorders as diverse as amyotrophic lateral sclerosis, Emery-Dreifuss muscular dystrophy and myasthenia gravis (Perez-Garcia & Burden, 2012; Pratt *et al.*, 2013; Arimura *et al.*, 2014; Ghazanfari *et al.*, 2015; Miyoshi *et al.*, 2017). These reports highlight the need to explore the effects of elevated MuSK pathway function upon skeletal muscle physiology and pathophysiology. We injected AAV encoding MuSK-GFP into the mouse TA muscle at 8-weeks postnatal. This resulted in ectopic expression of MuSK-GFP throughout the sarcolemma. We report three novel effects of the expanded expression of MuSK: 1/ *mdx* muscles were made more resistant to the acute EC-induced loss of strength; 2/ *mdx* muscles revealed reductions in the size of their NMJs; 3/ both wild-type and *mdx* muscles developed a decay in nerve-evoked contraction force during tetanus.

Wild-type muscles overexpressing MuSK-GFP revealed an unexpected decrement in nerve-evoked force production during a 400msec maximum tetanus (effect size 1.8). This effect was also found in *mdx* mice. It was not replicated by rapsyn-GFP. Force evoked by direct stimulation of the muscle was not affected by MuSK-GFP, suggesting that MuSK was acting

upstream of excitation-contraction coupling to produce a progressive failure of neuromuscular transmission during high frequency stimulation (150/sec). During any train of nerve stimuli there is a natural decay in the number of quanta of acetylcholine released by the nerve terminal (Kamenskaya *et al.*, 1975). In myasthenia gravis, reduced numbers of post-synaptic AChRs, combined with the natural decline in quantal content during tetanus, results in progressive failure of the endplate potential to reach threshold in the muscle fibres (Plomp *et al.*, 2015). In wild-type muscles we found no evidence that elevating MuSK caused a (myasthenia-like) reduction in the postsynaptic AChR density, nor any reduction in the total area of synaptic specializations at the NMJ (Fig 5). On the other hand, elevated MuSK might cause fatiguing failure of nerve-evoked force via subtle changes to other parameters of quantal neuromuscular transmission, or possibly via nerve conduction failure. A future intracellular electrophysiological study will be needed to clarify this effect of MuSK.

In *mdx* mice, the area of synaptic specializations per endplate was larger, and responded differently to MuSK-GFP, when compared to wild-type endplates. Studies in the diaphragm muscle of *mdx* mice have revealed subtle impairments to neuromuscular transmission (Nagel *et al.*, 1991 ; van der Pijl *et al.*, 2016). Accordingly, the larger synaptic area in *mdx* mice might result from adaptive growth of the synapse. In any event, injection of AAV-MuSK-GFP at 8-weeks seemed to reverse the enlargement of the NMJs in *mdx* mouse muscles (effect size=1.79). The effect of rapsyn-GFP on endplate AChR area was less substantial. Expression of MuSK-GFP in muscles of *mdx* mice also led to a reduction in the intensity of endplate AChR labelling. The 'synapse shrinking' effects of MuSK-GFP in *mdx* mouse muscles contrast sharply with the synapse-stabilizing effects of elevating MuSK expression/function in dystrophin-positive muscles (Kim & Burden, 2008; Arimura *et al.*, 2014; Ghazanfari *et al.*, 2015). MuSK acts via Src-family tyrosine kinases to phosphorylate and stabilize AChR clusters. However Shp2, a tyrosine phosphatase, also becomes activated downstream of MuSK, and it has an opposing effect. Depending upon the cellular/molecular context, the balance of kinase and phosphatase activities might favour either the growth or disassembly of AChR clusters (Ngo *et al.*, 2004; Trinidad & Cohen, 2004; Sadasivam *et al.*, 2005; Camilleri *et al.*, 2007; Ngo *et al.*, 2012). It has been proposed that, during development, MuSK activity at the incipient NMJ drives a spreading Shp2-mediated de-phosphorylation and disassembly of AChR clusters at distant (non-synaptic) sites on the same muscle cell (Qian *et al.*, 2008). We postulate that endplates lacking dystrophin (*mdx*) become

susceptible to a similar mechanism of AChR cluster dispersion driven by distant (extrasynaptic) MuSK. This possibility should be considered in developing potential MuSK-targeted therapies.

A key finding of the present study was that elevated MuSK expression reduced the susceptibility of *mdx* muscle to EC-induced loss of strength (effect size 1.57). Recent studies in *mdx* mice suggest that much of the acute drop in force that follows an EC challenge is due to failure of action potential generation in some of the muscle fibres. Pratt and colleagues proposed that the endplates of *mdx* mice might be prone to EC-induced damage (and neuromuscular transmission failure) due to relatively low expression of MuSK in their muscles. They reported that the drop in nerve-evoked force, after the mouse quadriceps muscle underwent a series of 15 ECs, was associated with a reduction in the magnitude of the compound muscle action potential (Pratt *et al.*, 2013). Our results, and those of others (Call *et al.*, 2013; Roy *et al.*, 2016), suggest that most of the loss of force after EC challenge occurs downstream of neuromuscular transmission per se. Following our EC challenge, nerve-evoked force fell to 69 (7)% of its initial value, but directly-evoked force fell to a comparable value (73 (6)%). Importantly, MuSK-GFP protected directly-evoked muscle force. *Mdx* muscles injected with AAV-MuSK-GFP retained 85 (3)% of their directly-evoked force after the EC challenge and 85 (5)% of their nerve-evoked force. Others have provided evidence ECs cause a loss of excitability in *mdx* muscle fibres, and that this helps to explain the acute loss of force (Call *et al.*, 2013; Roy *et al.*, 2016). Call et al. subjected the anterior crural muscles of *mdx* mice to 100 ECs *in vivo* and reported reduced compound muscle action potential magnitudes. They reported altered resting membrane potentials in many of the muscle fibres (partially depolarised), which could reduce excitability. Roy et al. showed that the decline in isometric force in the TA muscle during 9 or 12 ECs was directly correlated with decline in the compound muscle action potential magnitude (Roy *et al.*, 2016). Since we did not record muscle action potentials our results cannot distinguish whether the loss of force that we recorded after 4 ECs was due to failure of muscle fibre excitability, nor whether MuSK prevents a loss of excitability. Curves showing the increase twitch-force as muscle stimulus voltage was increased were not grossly different among treatment groups (Fig 9). However, these curves would not be expected to reveal fibres that may have become completely non-excitable. Such non-excitable fibres might well be responsible, in part or whole, for the drop in force after an EC challenge. The current findings suggest that MuSK

and rapsyn can have a protective effect that extends beyond the motor endplate and into the extrasynaptic sarcolemma of *mdx* muscle fibres.

In the absence of dystrophin, reduced sarcolemmal expression of β-dystroglycan and other DAPs in *mdx* muscles seems to contribute to the fragility of the dystrophic muscle fibres (Matsumura *et al.*, 1993; Johnson *et al.*, 2013; Rader *et al.*, 2016). In particular conditional knock-down of dystroglycan expression increased the susceptibility of healthy muscles to EC-induced loss of force (Rader *et al.*, 2016). Injection of AAV-MuSK-GFP into muscles of *mdx* mice led to increased expression of both MuSK and β-dystroglycan throughout the sarcolemma (Fig 6 & 7). Interestingly, the protective effect of MuSK-GFP was mimicked by rapsyn-GFP (Fig 3C), suggesting the involvement of the MuSK/rapsyn pathway. Activation of MuSK is known to stabilize rapsyn, increasing rapsyn levels in the cytoplasm (Brockhausen *et al.*, 2008; Luo *et al.*, 2008). In turn, rapsyn binds phosphorylated AChRs and stabilizes the endplate (Apel *et al.*, 1997; Gervásio & Phillips, 2005; Gervásio *et al.*, 2007; Borges *et al.*, 2008; Brockhausen *et al.*, 2008; Luo *et al.*, 2008; Ghazanfari *et al.*, 2011). The RING-H2 domain of rapsyn has been reported to function as an E3 ligase, covalently tagging AChRs with the ubiquitin-like protein, Nedd8, and thereby protecting AChRs from ubiquitin-mediated degradation (Li *et al.*, 2016). Rapsyn can also bind to β-dystroglycan (Cartaud *et al.*, 1998; Bartoli *et al.*, 2001). It is conceivable that, in *mdx* muscles, the MuSK-rapsyn pathway has the potential to restore stability to sarcolemmal β-dystroglycan by a similar mechanism.

MuSK might reduce muscle fibre fragility by increasing the expression of utrophin in the sarcolemma (Fig 8). Utrophin can protect sarcolemmal β-dystroglycan from ubiquitin-mediated degradation by binding to its cytoplasmic tail (Choa *et al.*, 2018). More importantly, interventions that increase the sarcolemmal expression of utrophin in animal models of DMD have been effective at reducing the number of degenerating muscle fibres and associated dystrophic pathologies (Guiraud *et al.*, 2018). *Mdx* muscles that had been injected with AAV-MuSK displayed markedly more intense sarcolemmal labelling for utrophin. Immunoblotting results were also consistent with an increase in utrophin (Fig 8). However additional experiments will be needed to quantify the changes in utrophin, the levels of other DAPs and muscle fibre integrity. Justin Fallon and colleagues have shown that biglycan (a basement membrane protein) can similarly increase utrophin

immunofluorescence in the sarcolemma and reduce EC-induced loss of force in muscles of *mdx* mice (Amenta *et al.*, 2011). Interestingly, they also found that biglycan binds to the extracellular domain of MuSK and potentiates the agrin-mediated activation of MuSK (Amenta *et al.*, 2012). Together these findings raise the possibility that treatments (such as biglycan and MuSK-GFP) that increase the expression or activity of MuSK may also help increase expression of utrophin in the dystrophin-deficient sarcolemma.

In addition to its tyrosine kinase signalling function, MuSK also moonlights as a co-receptor for bone morphogenetic protein-4. When MuSK is expressed in the muscle cell membrane, it binds to certain bone morphogenetic protein receptors (ALK3 & ALK6). MuSK can thereby modify the transcriptome of the muscle cell (Yilmaz *et al.*, 2016). Thus it is also possible that extrasynaptic MuSK might somehow tweak the gene expression profile of the *mdx* muscle fibres in a manner that helps protect them from EC challenge. Further detailed studies will be required to define the correct molecular mechanism.

In summary, injection of AAV encoding MuSK-GFP into the TA muscle of 8-week old *mdx* muscles caused broad sarcolemmal expression of MuSK, similar to the distribution of endogenous MuSK found in soleus muscle fibres (Punga *et al.*, 2011). This was associated with increased utrophin and β-dystroglycan immunolabelling of the sarcolemma, and improved retention of muscle strength after EC challenge. The acute reduction in muscle force following an EC challenge provides a useful measure of the particular fragility of dystrophic muscle fibres, but it does not equate to muscle fibre necrosis. Future studies should reveal the extent to which injecting AAV-MuSK into younger *mdx* mice can prevent the subsequent development of the full dystrophic phenotype. Our study is, we believe, the first to show that MuSK can act beyond the NMJ to help protect dystrophic muscles from injury-induced loss of strength. The expression level, and cellular distribution of endogenous MuSK varies substantially among different skeletal muscles of the body (Punga *et al.*, 2011). Further investigation of the extrasynaptic functions of MuSK might help to clarify why particular muscle groups are more affected in particular human neuromuscular diseases.

Additional information section

Competing Interests

The authors have no competing interests in relation to this manuscript.

Funding

This work was funded by Bridging Grants from The University of Sydney to WDP (2015, 2016 & 2017). ST was supported by a NHMRC Program grant to DA (573732).

Author contributions

WDP, ST, DA and PG contributed to conception and design of the work. ST, JB, MM, JH and WDP contributed to the acquisition, analysis or interpretation of the data. All authors contributed to drafting the work or revising it critically for important intellectual content. All authors approved the final version of the manuscript and agree to be accountable for all aspects of the work in ensuring that questions related to the accuracy or integrity of any part of the work are appropriately investigated and resolved. All persons designated as authors qualify for authorship, and all those who qualify for authorship are listed.

Acknowledgments

We would like to thank Drs Stephen W Reddel and Peter G Noakes for valuable discussions, Dr Louise Cole (Bosch Institute Advanced Microscopy Facility), Dr Donna Lai and Dr Sheng Hua (Bosch Institute Molecular Biology Facility) for technical support and Dr Hongwei Qian (Baker Heart and Diabetes Institute, and The University of Melbourne) for assistance with the production of the recombinant AAV vectors.

References

Adams ME, Kramarcy N, Krall SP, Rossi SG, Rotundo RL, Sealock R & Froehner SC. (2000). Absence of α-syntrophin leads to structurally aberrant neuromuscular synapses deficient in utrophin. *J Cell Biol* **150,** 1385-1397.

Allen DG, Whitehead NP & Froehner SC. (2016). Absence of dystrophin disrupts skeletal muscle signalling: roles of Ca^{2+}, reactive oxygen species, and nitric oxide in the development of muscular dystrophy *Physiol Rev* **96,** 253–305.

Amenta AR, Creely HE, Mercado ML, Hagiwara H, McKechnie BA, Lechner BE, Rossi SG, Wang Q, Owens RT, Marrero E, Mei L, Hoch W, Young MF, McQuillan DJ, Rotundo RL & Fallon JR. (2012). Biglycan is an extracellular MuSK binding protein important for synapse stability *J Neurosci* **32,** 2324-2334.

Amenta AR, Yilmaz A, Bogdanovich S, McKechnie BA, Abedi M, Khurana TS & Fallon JR. (2011). Biglycan recruits utrophin to the sarcolemma and counters dystrophic pathology in mdx mice. *Proc Natl Acad Sci U S A* **108,** 762-767. .

Apel ED, Glass DJ, Moscoso LM, Yancopoulos GD & Sanes JR. (1997). Rapsyn is required for MuSK signaling and recruits synaptic components to a MuSK-containing scaffold. *Neuron* **18,** 623-635.

Arimura S, Okada T, Tezuka T, Chiyo T, Kasahara Y, Yoshimura T, Motomura M, Yoshida N, Beeson D, Takeda S & Yamanashi Y. (2014). Neuromuscular disease. DOK7 gene therapy benefits mouse models of diseases characterized by defects in the neuromuscular junction. *Science* **345,** 1505-1508.

Ayalon G, Davis JQ, Scotland PB & Bennett V. (2008). An ankyrin-based mechanism for funcitonal organization of dytrophin and dystroglycan. *Cell* **135,** 1189-1200.

Barresi R & Campbell KP. (2006). Dystroglycan: from biosynthesis to pathogenesis of human disease. *J Cell Sci* **119,** 199-207.

Bartoli M, Ramarao MK & Cohen JB. (2001). Interactions of the rapsyn RING-H2 domain with dystroglycan. *J Biol Chem* **276,** 24911-24917.

Bergamin E, Hallock PT, Burden SJ & Hubbard SR. (2010). The cytoplasmic adaptor protein Dok7 activates the receptor tyrosine kinase MuSK via dimerization. *Mol Cell* **39,** 100-109.

Blankinship MJ, Gregorevic P, Allen JM, Harper SQ, Harper H, Halbert CL, Miller D & Chamberlain JS. (2004). Efficient Transduction of Skeletal Muscle Using Vectors Based on Adeno-associated Virus Serotype 6. *Mol Therapy* **10,** 671-678.

Borges L, Yechikov S, Lee YI, Rudell JB, Friese MB, Burden SJ & Ferns M. (2008). Identification of a motif in the acetylcholine receptor β-subunit whose phosphorylation regulates rapsyn association and postsynaptic receptor localization. *J Neurosci* **28,** 11468-11476.

Brockhausen J, Cole RN, Gervásio OL, Ngo ST, Noakes PG & Phillips WD. (2008). Neural agrin increases postsynaptic ACh receptor packing by elevating rapsyn protein at the mouse neuromuscular synapse. *Dev Neurobiol* **68,** 1153-1169.

Brussee V, Tardif F & Tremblay JP. (1997). Muscle fibers of *mdx* mice are more vulnerable to exercise than those of normal mice. *Neuromuscul Disord* **7,** 487-492.

Call JA, Warren GL, Verma M & Lowe DA. (2013). Acute failure of action potential conduction in *mdx* muscle reveals a new mechanism of contraction-induced force loss. *J Physiol* **591,** 3765-3776.

Camilleri AA, Willmann R, Sadasivam G, Lin S, Rueff MA, Gesemann M & Fuhrer C. (2007). Tyrosine phosphatases such as SHP-2 act in balance with Src-family kinases in stabilization of postsynaptic clusters of acetylcholine receptors. *BMC Neurosci* **8,** 46.

Carlson CG & Roshek DM. (2001). Adult dystrophic (*mdx*) endplates exhibit reduced quantal size and enhanced quantal variation. *Pflugers Arch* **442,** 369-375.

Carnwath JW & Shotton DM. (1987). Muscular dystrophy in the *mdx* mouse: histopathology of the soleus and extensor digitorum longus muscles. *J Neurol Sci* **80,** 39-54.

Cartaud A, Coutant S, Petrucci TC & Cartaud J. (1998). Evidence for in situ and *in vitro* association between β-dystroglycan and the subsynaptic 43K rapsyn protein. *J Biol Chem* **273,** 11321-11326.

Cheng A, Morsch M, Murata Y, Ghazanfari N, Reddel SW & Phillips WD. (2013). Sequence of age-associated changes to the mouse neuromuscular junction and the protective effects of voluntary exercise. *PLoS One* **8,** e67970.

Choa E-B, Yooa W, Yoonb SK & Yoon J-B. (2018). β-dystroglycan is regulated by a balance between WWP1-mediated degradation and protection from WWP1 by dystrophin and utrophin. *BBA - Molecular Basis of Disease* **1864** 2199–2213.

Cole RN, Ghazanfari N, Ngo ST, Gervasio OL, Reddel SW & Phillips WD. (2010). Patient autoantibodies deplete postsynaptic Muscle Specific Kinase leading to disassembly of the ACh receptor scaffold and myasthenia gravis in mice. *J Physiol* **588.17,** 3217-3229.

DeChiara TM, Bowen DC, Valenzuela DM, Simmons MV, Poueymirou WT, Thomas S, Kinetz E, Compton DL, Rojas E, Park JS, Smith C, DiStefano PS, Glass DJ, Burden SJ & Yancopoulos GD. (1996). The receptor tyrosine kinase MuSK is required for neuromuscular junction formation *in vivo*. *Cell* **85,** 501-512.

Deconinck AE, Potter AC, Tinsley JM, Wood SJ, Vater R, Young C, Metzinger L, Vincent A, Slater CR & Davies KE. (1997). Postsynaptic abnormalities at the neuromuscular junctions of utrophin-deficient mice. *J Cell Biol* **136,** 883-894.

Dellorusso C, Crawford RW, Chamberlain JS & Brooks SV. (2001). Tibialis anterior muscles in *mdx* mice are highly susceptible to contraction-induced injury. *J Muscle Res Cell Motil* **22,** 467-475.

Duddy W, Duguez S, Johnston H, Cohen TV, Phadke A, Gordish-Dressman H, Nagaraju K, Gnocchi V, Low SH & Partridge T. (2015). Muscular dystrophy in the *mdx* mouse is a severe myopathy compounded by hypotrophy, hypertrophy and hyperplasia. *Skel Muscle* **5,** 16.

Faber RM, Hall JK, Chamberlain JS & Banks GB. (2014). Myofiber branching rather than myofiber hyperplasia contributes to muscle hypertrophy in *mdx* mice. *Skelet Muscle* **4,** 10.

Gervásio OL, Armson PF & Phillips WD. (2007). Developmental increase in the amount of rapsyn per acetylcholine receptor promotes postsynaptic receptor packing and stability. *Dev Biol* **305,** 262-275.

Gervásio OL & Phillips WD. (2005). Increased ratio of rapsyn to ACh receptor stabilizes postsynaptic receptors at the mouse neuromuscular synapse. *J Physiol* **562.3,** 673-685.

Ghazanfari N, Fernandez KJ, Murata Y, Morsch M, Ngo ST, Reddel SW, Noakes PG & Phillips WD. (2011). Muscle Specific Kinase: Organiser of synaptic membrane domains. *Int J Biochem Cell Biol* **43,** 295-298.

Ghazanfari N, Linsao ELTB, Trajanovska S, Morsch M, Gregorevic P, Liang SX, Reddel SW & Phillips WD. (2015). Forced expression of muscle specific kinase slows postsynaptic acetylcholine receptor loss in a mouse model of MuSK myasthenia gravis. *Physiol Rep* **3,** 12658.

Ghazanfari N, Morsch M, Reddel SW, Liang SX & Phillips WD. (2014). Muscle Specific Kinase autoantibodies suppress the MuSK pathway and ACh receptor retention at the mouse neuromuscular junction. *J Physiol* **592,** 2881-2897.

Grounds MD, Radleya HG, Lynch GS, Nagaraju K & De Luca A. (2008). Towards developing standard operating procedures for pre-clinical testing in the *mdx* mouse model of Duchenne muscular dystrophy. *Neurobiology of Disease* **31,** 1-19.

Guiraud S, Roblin D & Davies EK. (2018). The potential of utrophin modulators for the treatment of Duchenne muscular dystrophy. *Expert Opinion on Orphan Drugs* **6,** 179–192.

Gumerson JD & Michele DE. (2011). The Dystrophin-Glycoprotein Complex in the Prevention of Muscle Damage. *J Biomed Biotechnol* **2011,** 210797. .

Johnson EK, Li B, Yoon JH, Flanigan KM, Martin PT, Ervasti J & Montanaro M. (2013). Identification of new dystroglycan complexes in skeletal muscle. *PLoS ONE* **8,** e73224. .

Kamenskaya MA, Elmqvist D & Thesleff S. (1975). Guanidine and neuromuscular transmission. II. Effect on transmitter release in response to repetitive nerve stimulation. *Arch Neurol* **32,** 510-518.

Kim N & Burden SJ. (2008). MuSK controls where motor axons grow and form synapses. *Nat Neurosci* **11,** 19-27.

Kim N, Stiegler AL, Cameron TO, Hallock PT, Gomez AM, Huang JH, Hubbard SR, Dustin ML & Burden SJ. (2008). Lrp4 is a receptor for agrin and forms a complex with MuSK. *Cell* **135,** 334-342.

Kiriaev L, Kueh S, Morley JW, North KN, Houweling PJ & Head SI. (2018). Branched fibers from old fast-twitch dystrophic muscles are the sites of terminal damage in muscular dystrophy. *Am J Physiol Cell Physiol* **314,** C662–C674.

Li L, Cao Y, Wu H, Ye X, Zhu Z, Xing G, Shen C, Barik A, Zhang B, Xie X, Zhi W, Gan L, Su H, Xiong WC & Mei L. (2016). Enzymatic Activity of the Scaffold Protein Rapsyn for Synapse Formation. *Neuron* **92,** 1–13.

Luo S, Zhang B, Dong X, Tao Y, Ting A, Zhou Z, Meixiong J, Luo J, Chiu FCA, Xiong WC & Mei L. (2008). HSP90β regulates rapsyn turnover and subsequent AchR cluster formation and maintenance. *Neuron* **60,** 97-110.

Lyons PR & Slater CR. (1991). Structure and function of the neuromuscular junction in young adult *mdx* mice. *J Neurocytol* **20,** 969-981.

Manning J & O'Malley D. (2015). What has the *mdx* mouse model of duchenne muscular dystrophy contributed to our understanding of this disease? *J Muscle Res Cell Motil* **36,** 155-167.

Matsumura K, Lee CC, Caskey CT & Campbell KP. (1993). Restoration of dystrophin-associated proteins in skeletal muscle of *mdx* mice transgenic for dystrophin gene. *FEBS Lett* **320,** 276-280.

McGeachie JK, Grounds MD, Partridge TA & Morgan JE. (1993). Age-related changes in replication of myogenic cells in *mdx* mice: quantitative autoradiographic studies. *J Neurolog Sci* **119,** 169-179.

Miyoshi S, Tezuka T, Arimura S, Tomono T, Okada T & Yamanashi Y. (2017). DOK7 gene therapy enhances motor activity and life span in ALS model mice. *EMBO Molecular Medicine* **e201607298**.

Nagel A, Lehmann-Horn F & Engel AG. (1991). Neuromuscular transmission in the *mdx* mouse. *Muscle Nerve* **13,** 742-749.

Ngo ST, Balke C, Phillips WD & Noakes PG. (2004). Neuregulin potentiates agrin-induced acetylcholine receptor clustering in myotubes. *Neuroreport* **15,** 2501-2505.

Ngo ST, Cole RN, Sunn N, Phillips WD & Noakes PG. (2012). Neuregulin-1 Potentiates Agrin-Induced Acetylcholine Receptor Clustering via Muscle Specific Kinase Phosphorylation. *J Cell Sci* **125,** 1531-1543.

Ohlendieck K & Campbell KP. (1991). Dystrophin-associated proteins are greatly reduced in skeletal muscle from *mdx* mice. *J Cell Biol* **115,** 1685-1694.

Pereboev AV, Ahmed N, thi Man N & Morris GE. (2001). Epitopes in the interacting regions of L-dystroglycan (PPxY motif) and dystrophin (WW domain). *Biochim Biophys Acta* **1527,** 54-60.

Perez-Garcia MJ & Burden SJ. (2012). Increasing MuSK Activity Delays Denervation and Improves Motor Function in ALS Mice. *Cell Rep* **2,** 1-6.

Plomp JJ, Morsch M, Phillips WD & Verschuuren JJGM. (2015). Electrophysiological analysis of neuromuscular synaptic function in myasthenia gravis patients and animal models *Exp Neurol* **270,** 41-54.

Pratt SJ, Shah SB, Ward CW, Inacio MP, Stains JP & Lovering RM. (2013). Effects of *in vivo* injury on the neuromuscular junction in healthy and dystrophic muscles. *J Physiol* **591,** 559-570.

Pratt SJ, Shah SB, Ward CW, Kerr JP, Stains JP & Lovering RM. (2015a). Recovery of altered neuromuscular junction morphology and muscle function in *mdx* mice after injury. *Cell Mol Life Sci* **72,** 153-164.

Pratt SJ, Valencia AP, Le GK, Shah SB & Lovering RM. (2015b). Pre- and postsynaptic changes in the neuromuscular junction in dystrophic mice. *Front Physiol* **6,** 252.

Punga AR, Maj M, Lin S, Meinen S & Rüegg MA. (2011). MuSK levels differ between adult skeletal muscles and influence postsynaptic plasticity. *Eur J Neurosci* **33,** 890-898.

Qian YK, Chan AWS, Madhavan R & Peng HB. (2008). The function of Shp2 tyrosine phosphatase in the dispersal of acetylcholine receptor clusters. *BMC Neurosci* **9,** 70.

Rader EP, Turka R, Willera Y, Beltrána D, Inamoria K, Petersona TA, Englea J, Proutya S, Matsumuraf K, Saitof F, Andersona ME & Campbell KP. (2016). Role of dystroglycan in limiting contraction-induced injury to the sarcomeric cytoskeleton of mature skeletal muscle. *Proc Natl Acad Sci U S A* **113,** 10992–10997.

Roy P, Rau F, Ochala J, Messéant J, Fraysse B, Lainé J, Agbulut O, Butler-Browne G, Furling D & Ferry A. (2016). Dystrophin restoration therapy improves both the reduced excitability and the force drop induced by lengthening contractions in dystrophic *mdx* skeletal muscle. *Skel Muscle* **6,** 23.

Ryder S, Leadley RM, Armstrong N, Westwood M, de Kock S, Butt T, Jain M & Kleijnen J. (2017). The burden, epidemiology, costs and treatment for Duchenne muscular dystrophy: an evidence review. *Orphanet J Rare Dis* **12,** 79. .

Sadasivam G, Willman R, Lin S, Erb-Vogtli S, Kong XC, Ruegg MA & Fuhrer C. (2005). Src-family kinases stabilize the neuromuscular synapse via protein interactions, phosphorylation, and cytoskeletal linkage. *J Neurosci* **25,** 10479-10493. .

Trinidad JC & Cohen JB. (2004). Neuregulin inhibits acetylcholine receptor aggregation in myotubes. *J Biol Chem* **279,** 31622-31628.

Tse N, Morsch M, Ghazanfari N, Cole L, Visvanathan A, Leamey C & Phillips WD. (2014). The neuromuscular junction: Measuring synapse size, fragmentation and changes in synaptic protein density using confocal fluorescence microscopy *J Visualized Exp* **94,** e52220.

Valenzuela DM, Stitt TN, DiStefano PS, Rojas E, Mattsson K, Compton DL, Nunez L, Park JS, Stark JL, Gies DR, Thomas S, Le Beau MM, Fernald AA, Copeland NG, Jenkins NA, Burden SJ, Glass DJ & Yancopoulos GD. (1995). Receptor tyrosine kinase specific for the skeletal muscle lineage: expression in embryonic muscle, at the neuromuscular junction, and after injury. *Neuron* **15,** 573-584.

van der Pijl EM, van Putten M, Niks EH, Verschuuren JJGM, Aartsma-Rus A & Plomp JJ. (2016). Characterization of neuromuscular synapse function abnormalities in multiple Duchenne muscular dystrophy mouse models. *Eur J Neurosci* **43,** 1623-1635. .

Whitehead NP, Streamer M, Lusambili LI, Sachs F & Allen DG. (2006). Streptomycin reduces stretch-induced membrane permeability in muscles from *mdx* mice. *Neuromuscul Disord* **16,** 845-854.

Willmann R, De Luca A, Benatar M, Grounds M, Dubach J, Raymackers JM, Nagaraju K & Network. R-NN. (2012). Enhancing translation: guidelines for standard pre-clinical experiments in *mdx* mice. *Neuromuscul Disord* **22,** 43-49. .

Yilmaz A, Kattamuri C, Ozdeslik RN, Schmiedel C, Mentzer S, Schorl C, Oancea E, Thompson TB & Fallon JR. (2016). MuSK is a BMP co-receptor that shapes BMP responses and calcium signaling in muscle cells. *Sci Sig* **9,** ra87.

Yiu EM & Kornberg AJ. (2015). Duchenne muscular dystrophy. *J Paediatr Child Health* **51,** 759-764. .

Zhang B, Luo S, Wang Q, Suzuki T, Xiong WC & Mei L. (2008). LRP4 Serves as a Coreceptor of Agrin *Neuron* **60,** 285-297.

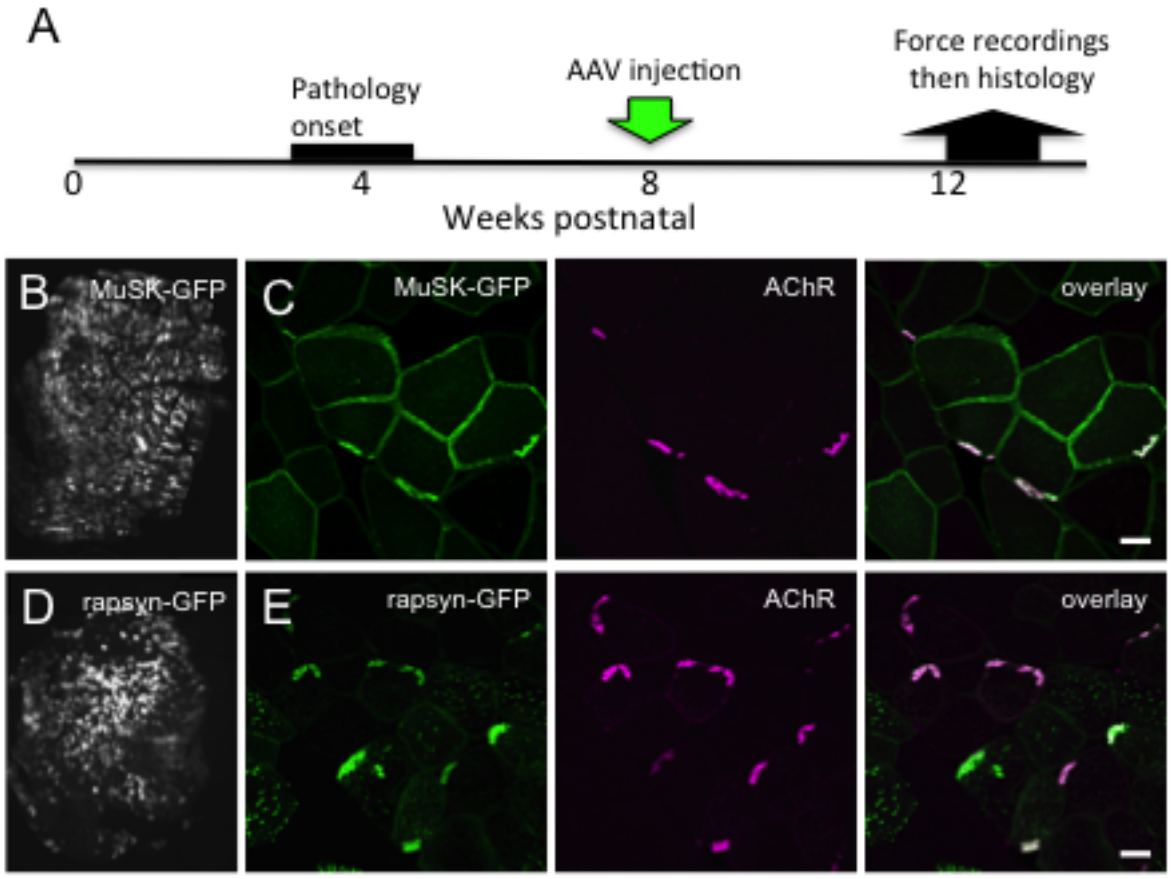

Fig 1 Intramuscular injection of recombinant AAV and expression of MuSK-GFP and rapsyn-GFP. **(A)** Experimental timeline. The TA muscle was injected with AAV encoding MuSK-GFP or rapsyn-GFP at 8-weeks of age and mice were killed for analysis 34 (5) days later. Contralateral control muscles were injected with empty AAV vector. An intense period of widespread muscle fibre necrosis begins at 3-weeks of age in *mdx* mice. **(B)** Whole transverse section through the TA muscle of a wild-type mouse showing widespread MuSK-GFP fluorescence. **(C)** Higher magnification showing localization of MuSK-GFP at AChR-rich motor endplates but also in the extrasynaptic sarcolemma. **(D)** Whole transverse section showing a broad distribution of rapsyn-GFP fluorescence across a wild-type muscle. **(E)** Rapsyn-GFP concentrated at the AChR-rich motor endplate. Scale bar for panels C & E is 20μm.

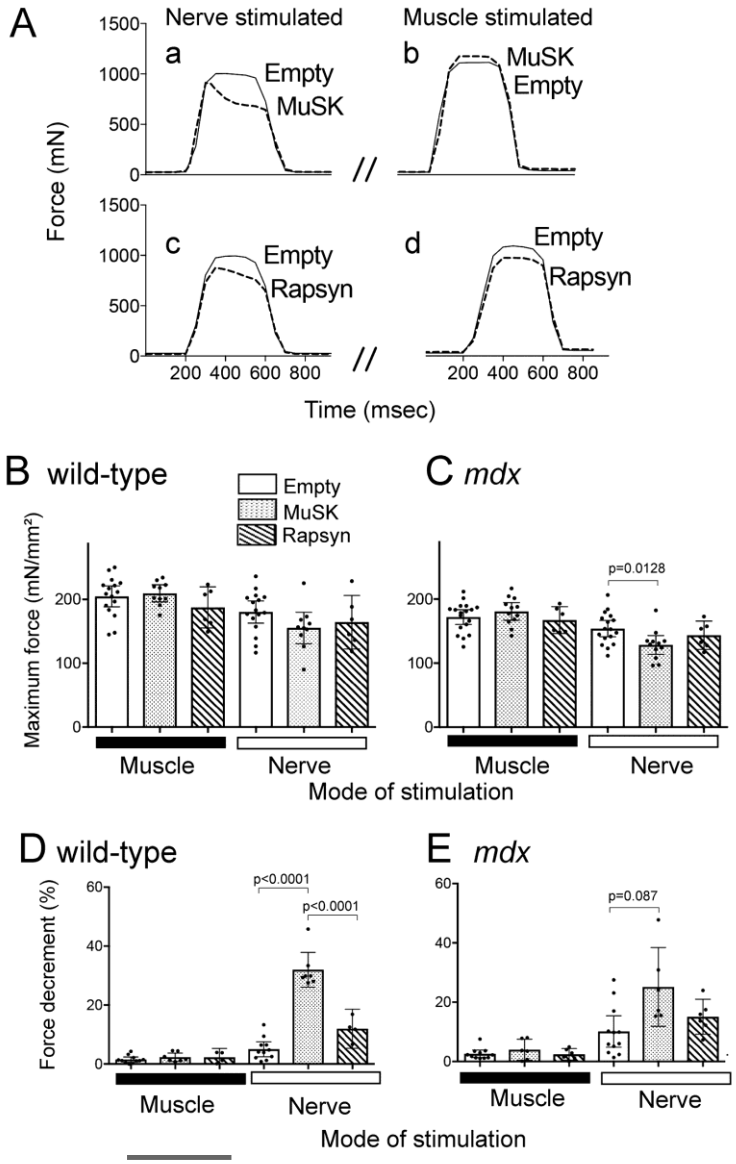

Fig 2 MuSK-GFP causes decrement in nerve-evoked force. **(Aa)** Sample isometric force traces revealing a decrement in nerve-evoked muscle force in a wild-type muscle expressing MuSK-GFP (dashed trace). No such decrement was evident in the contralateral empty-vector muscle (solid trace). **(Ab)** Direct electrical stimulation of the same muscles yielded steady isometric force. **(Ac)** Nerve-evoked tetanus from a wild-type muscle expressing rapsyn-GFP (dashed trace) and contralateral empty-vector control muscle (solid trace). **(Ad)** Force produced by direct electrical stimulation of the same muscles as in Ac. **(B)** Quantitation of maximum force generated by wild-type muscles expressing MuSK-GFP (stippled bars), rapsyn-GFP (hatched bars) and empty-vector control muscles (open bars). Muscles were stimulated directly ('Muscle') or via the nerve (Nerve') as indicated. **(C)** Maximum force results for *mdx* muscles. **(D)** Percentage force decrement for wild-type muscles during a 400 msec tetanus. **(E)** Percentage force decrement for *mdx* muscles. Symbols represent individual muscles while bars indicate means and 95% confidence intervals. One-way ANOVA with Tukey's multiple comparisons post-tests were used to compare among MuSK, rapsyn and empty vector control muscles for responses to direct muscle stimulation, and separately for their responses to nerve-stimulation (p-values less than 0.05 are indicated above the bars).

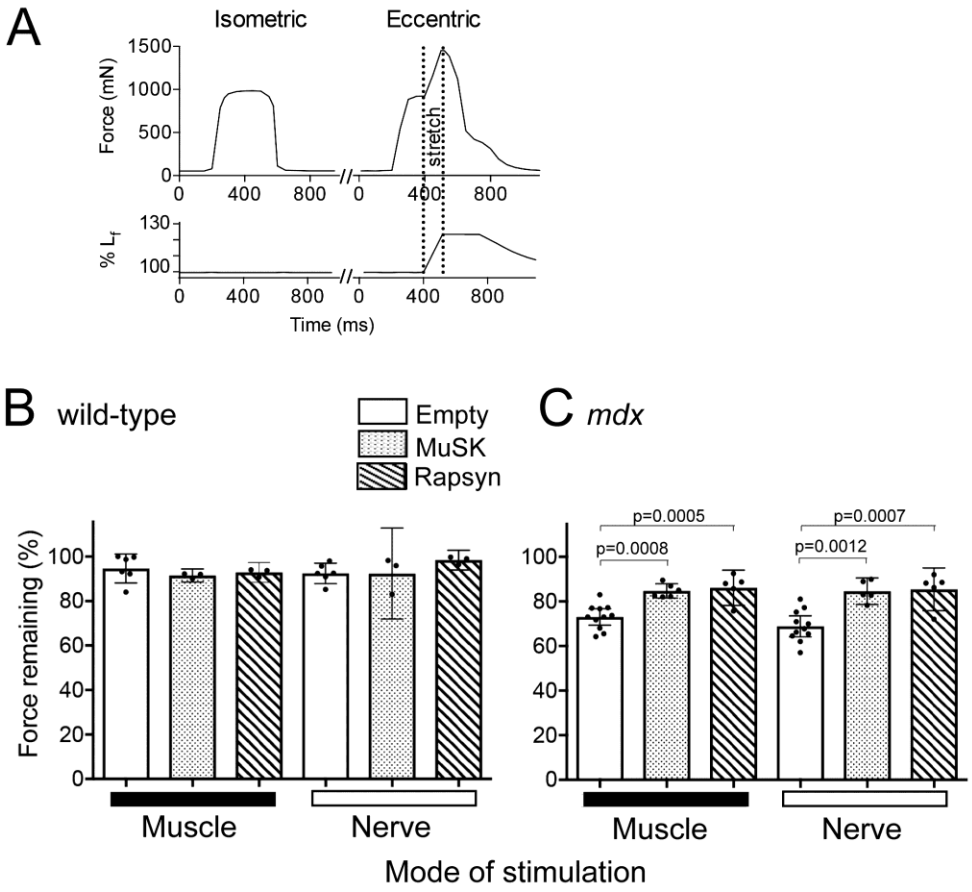

Fig 3 MuSK-GFP and rapsyn-GFP help protect *mdx* muscles against acute EC-induced loss of strength. **(A)** Sample traces illustrate isometric and eccentric contractions of the TA muscle in anaesthetized mice. The upper traces show tension recorded by the force transducer. For the ECs, the servomotor device imposed a controlled muscle lengthening beginning halfway through the maximal tetanic activation. The lower traces shows length changes, relative to optimal fibre length (L_f). Muscles were stimulated directly during each EC. **(B & C)** Isometric force remaining after a series of four ECs, expressed as a percentage of force immediately before the EC challenge (initial force). **(B)** Wild-type muscles retained nearly all their initial force after EC challenge. **(C)** *Mdx* empty-vector control muscles retained less of their original force after the EC challenge (open bars). *Mdx* muscles expressing either MuSK-GFP or rapsyn-GFP retained significantly more of their initial force (stippled and hatched bars respectively). Symbols represent individual muscles while bars indicate the means and 95% confidence intervals. One-way ANOVA with Tukey's multiple comparisons post-tests were used to compare among MuSK, rapsyn and empty vector control muscles for responses to direct muscle stimulation, and separately for responses to nerve-stimulation (p-values less than 0.05 are indicated above the bars).

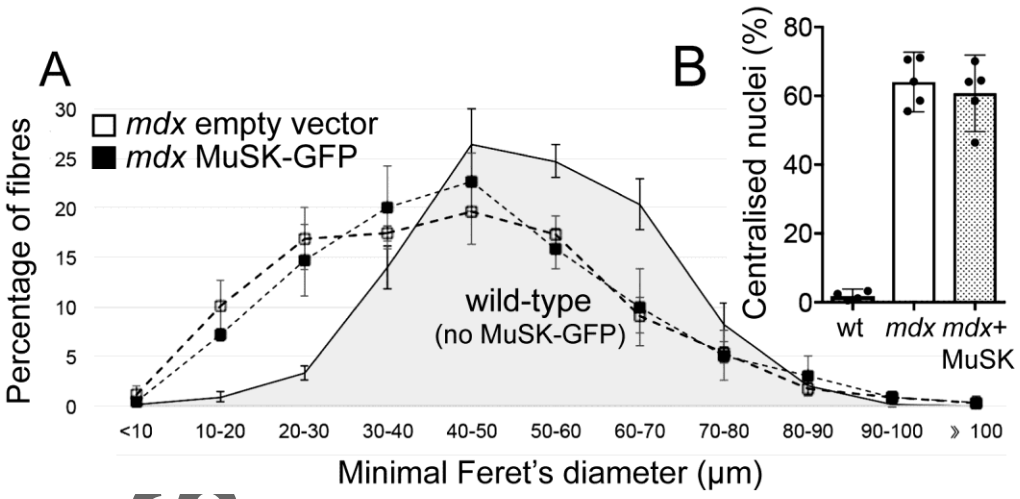

Fig 4 Quantitation of muscle fibre pathology. **(A)** Frequency distributions of girth (minimal Feret's diameter) of muscle fibres. Filled squares show results for *mdx* muscles injected with AAV-MuSK-GFP while open circles show results from contralateral empty–vector control muscles. The shaded distribution represents untreated wild-type muscles. Symbols show the means while bars indicate 95% confidence intervals for n=4 wild-type muscles and n=5 *mdx* muscles. **(B)** Percentage of muscle fibre profiles displaying at least one centralised nucleus. Symbols represent the percentage for each sampled muscle.

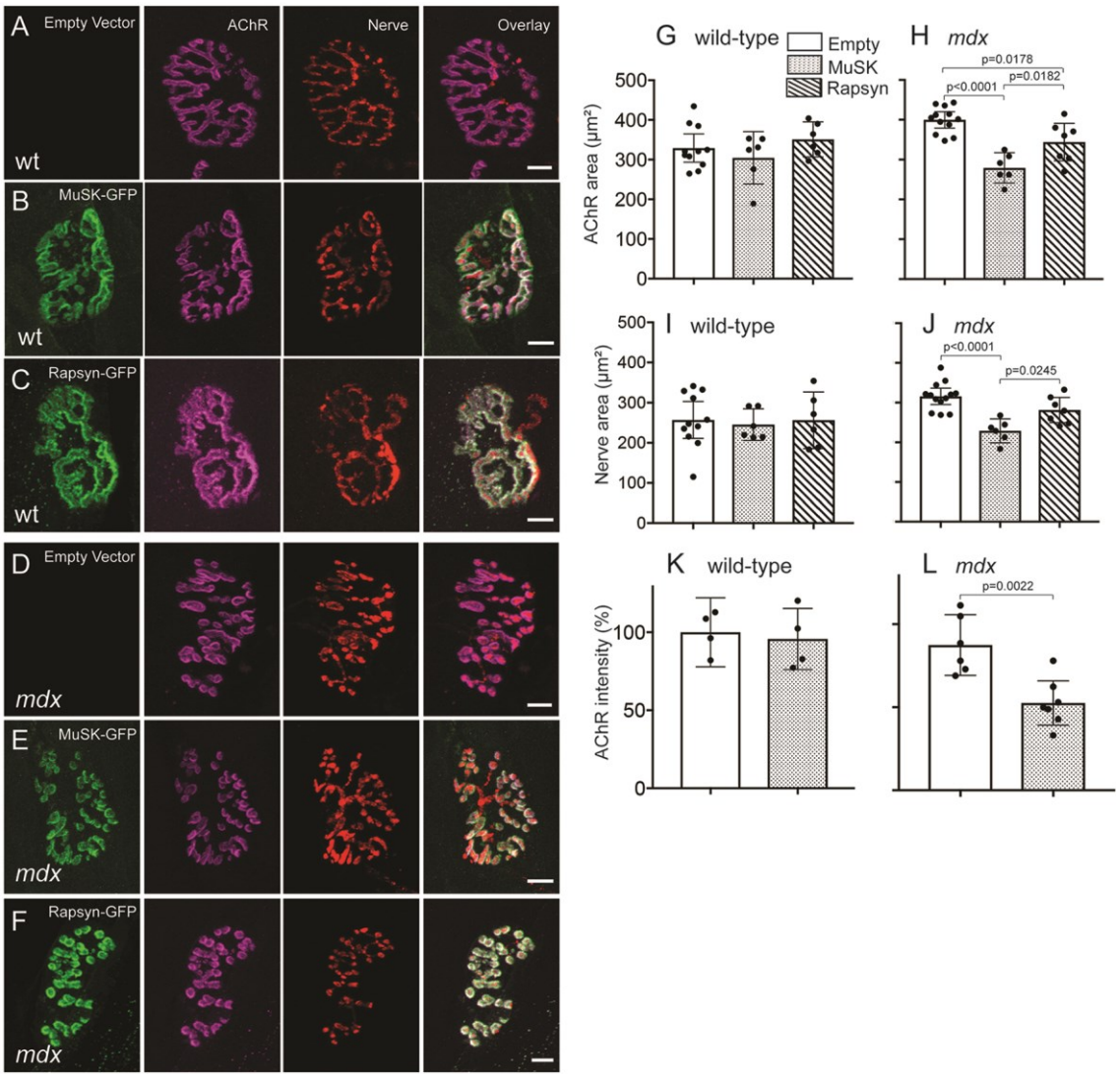

Fig 5 Effects of MuSK-GFP and rapsyn-GFP upon endplate size. **(A-C)** Exemplar enface images of NMJs from wild-type mouse TA muscles injected with empty AAV vector (A), AAV encoding MuSK-GFP (B) or AAV encoding rapsyn-GFP (C). Confocal maximum projection Z-stack images of endplates show GFP fluorescence (first column), AChR labelling (second column), anti-synaptophysin labelling ("nerve"; third column) and an overlay of all the fluorescence channels (fourth column). **(D-F)** NMJs from *mdx* muscles injected with empty AAV vector, MuSK-GFP or rapsyn-GFP. Scale bars =10 µm. **(G-J)** Quantitation of the total area of AChR and presynaptic nerve terminal (synaptophysin) per endplate. Results for muscles fixed either before or after EC challenge (Table I) were pooled for these graphs. **(G)** Endplate AChR area for wild-type muscles. **(H)** Endplate AChR area for *mdx* muscles. **(I)** Nerve terminal area at wild-type endplates. **(J)** Nerve terminal area at *mdx* endplates. For panels G-J, one-way ANOVA with Tukey's post-test was used to test for differences among the means for each treatment group. **(K & L)** Effect of MuSK-GFP upon the intensity of endplate AChR labelling, as assessed from transverse sections in a follow-up experiment. **(K)** In wild-type muscles, MuSK-GFP had no effect upon the intensity of endplate AChR labelling. **(L)** In *mdx* muscles expressing MuSK-GFP, the intensity of endplate AChR labelling was lower than for contralateral empty-vector control muscles (two-sided unpaired Student's t-test). Bars show the mean and 95% confidence intervals. Symbols represent individual muscles.

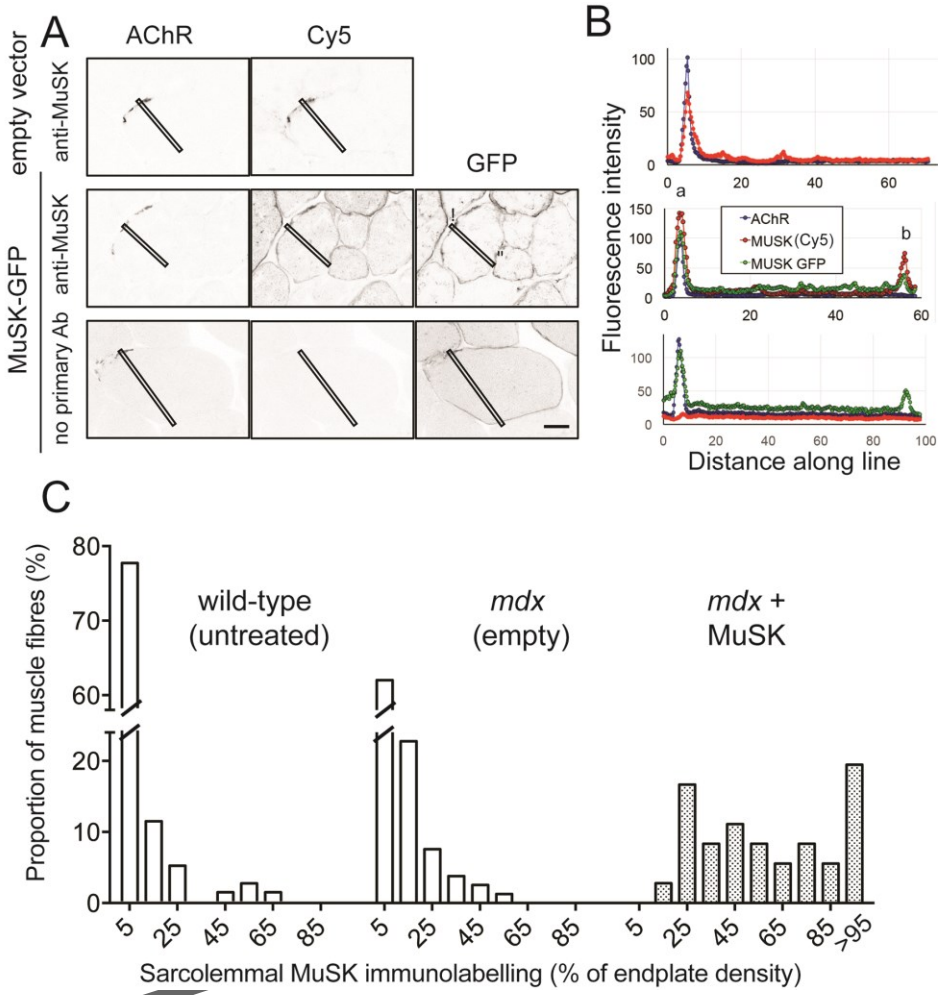

Fig 6 AAV-MuSK-GFP causes sarcolemmal expression of MuSK. **(A)** Transverse sections through *mdx* control muscles show the subcellular distribution of AChR (Alexa555-α-bungarotoxin), anti-MuSK immunofluorescence (with Cy5 secondary antibody) and GFP fluorescence. To facilitate reproduction, the image intensity scale was inverted, such that the brightest fluorescence is seen as dark on a light background. Top row: *mdx* empty-vector control muscle shows endogenous MuSK (Cy5 channel) restricted to the AChR-rich endplate. Middle row: *mdx* muscle expressing MuSK-GFP showing MuSK throughout the sarcolemma. Bottom row: *mdx* muscle expressing MuSK-GFP but with primary antibody left out of the staining procedure (negative control). Scale bar =25μm. **(B)** Fluorescence intensity plots corresponding to the line shown on the same row in panel A. The left hand peak in each case represents the motor endplate. The middle row trace shows two peaks of MuSK immunofluorescence: the motor endplate (a) and the extrasynaptic sarcolemma (b). **(C)** Frequency distributions comparing the intensity of MuSK immunolabelling in the sarcolemma as a percentage of the endplate value (peak b as a percentage of peak a). In *mdx* muscles injected with AAV encoding MuSK-GFP, most muscle fibres showed distinct anti-MuSK immunolabelling in their sarcolemma.

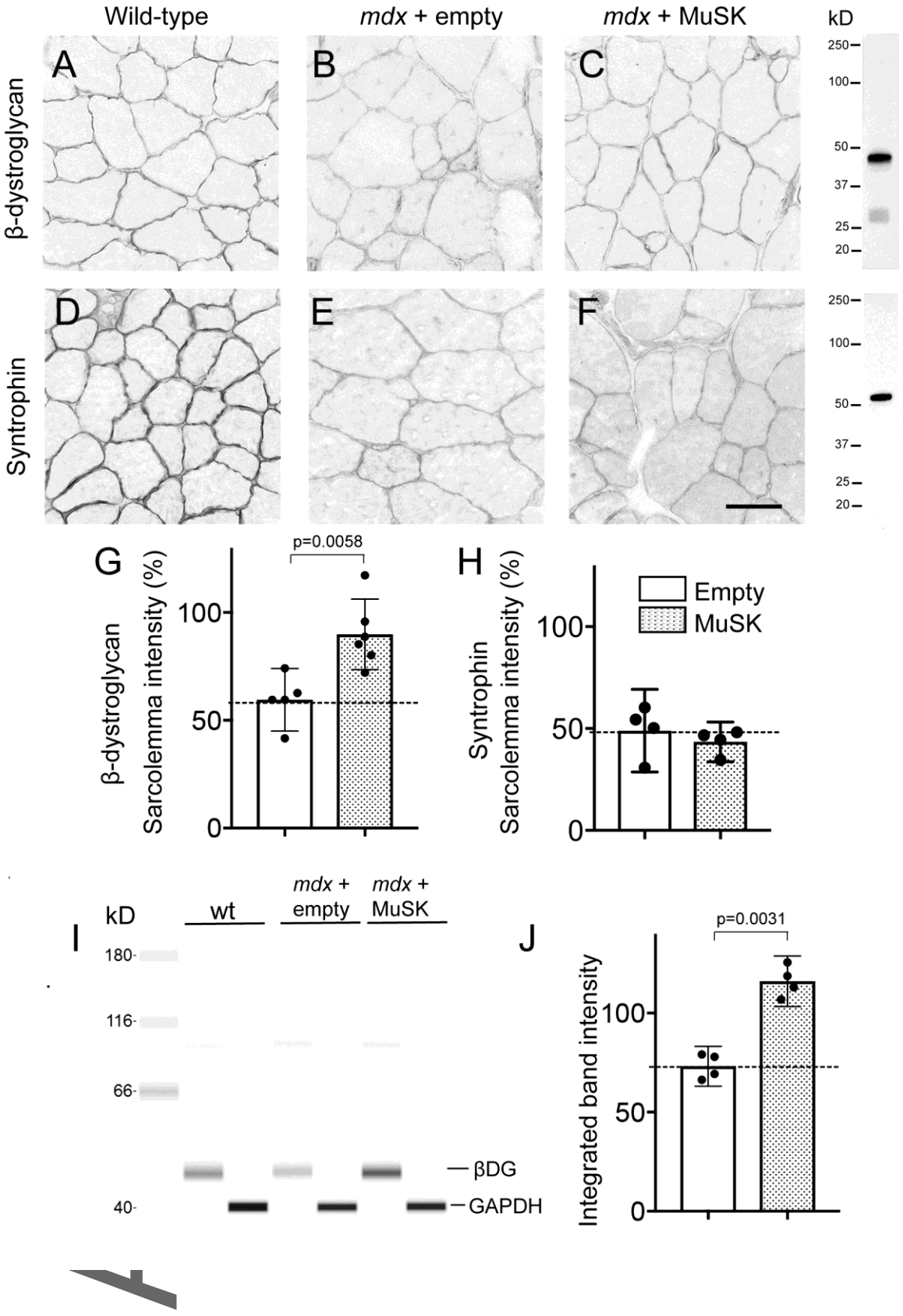

Fig 7 MuSK-GFP helps restore β-dystroglycan expression to *mdx* muscle fibres. **(A-C)** Immunofluorescent labelling for β-dystroglycan in transverse sections through untreated wild-type muscle (A), *mdx* empty-vector control muscle (B), and *mdx* muscle expressing

MuSK-GFP (C). The image intensity scale has been inverted such that the brightest fluorescence is seen as dark on a light background to facilitate reproduction. **(D-F)** Immunofluorescent labelling for α1-syntrophin in untreated wild-type muscle (D), *mdx* empty-vector control muscle (E), and *mdx* muscle expressing MuSK-GFP (F). Scale bar = 50μm. Western blot lanes to the right of panels C and F show expected bands for β-dystroglycan and α1-syntrophin respectively. **(G)** MuSK-GFP increased the intensity of β-dystroglycan immunofluorescence in the extrasynaptic sarcolemma of *mdx* muscles. **(H)** The sarcolemmal density of α1-syntrophin in *mdx* muscles was not affected by MuSK-GFP. Intensity values are expressed as a percentage of the mean for wild-type muscles. **(I)** Muscle proteins separated and probed for β-dystroglycan using the Wes™ automated capillary electrophoresis system. GAPDH loading controls were run in parallel capillaries (see *Methods*). Molecular weight markers are shown in the first lane. **(J)** Quantitation of β-dystroglycan protein levels. Band intensities were normalised to GAPDH. Bars show mean and 95% confidence intervals for *mdx* muscles expressing MuSK-GFP and contralateral empty vector control muscles expressed as a percentage of values for untreated wild-type muscles. Values for individual sample muscles are indicated by symbols (p-values <0.05 are shown; paired t-tests).

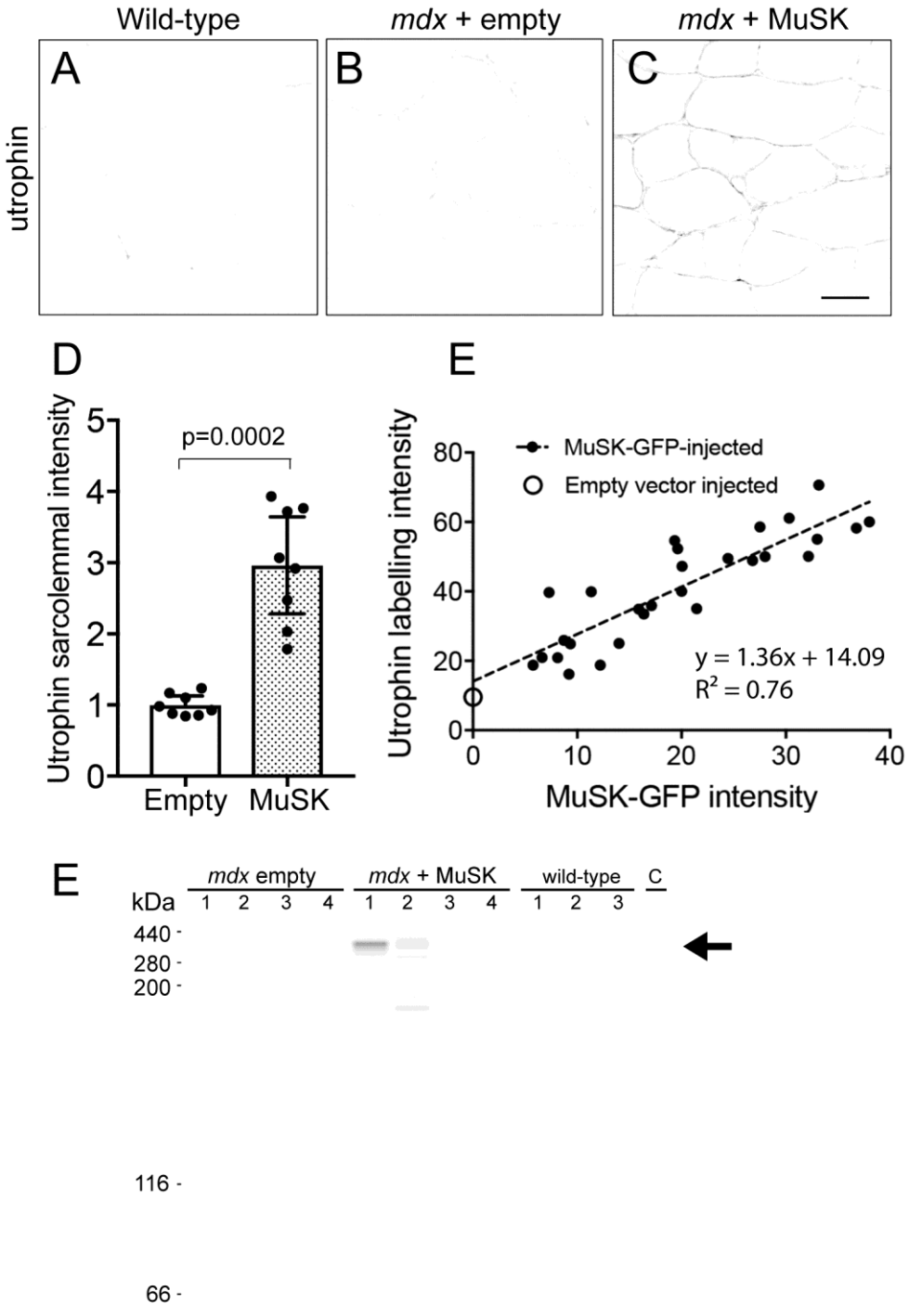

Fig 8 MuSK-GFP increases the intensity of utrophin immunolabelling of the sarcolemma of *mdx* muscle fibres. **(A-C)** Immunofluorescent labelling for utrophin in transverse sections through untreated wild-type muscle (A), *mdx* empty-vector control muscle (B), and *mdx* muscle expressing MuSK-GFP (C). The image intensity scale has been inverted such that the brightest fluorescence is seen as dark on a light background to facilitate reproduction. Scale bar = 50μm. **(D)** Muscles injected with AAV-MuSK-GFP revealed higher intensity of

utrophin immunofluorescence in the sarcolemma. Bars show mean and 95% confidence intervals for *mdx* muscles expressing MuSK-GFP, compared to contralateral, empty-vector control muscles. Values for individual sample muscles are indicated by symbols (P=0002; paired t-test). **(E)** Direct correlation between intensity of utrophin immunofluorescence in the sarcolemma and the corresponding intensity of MuSK-GFP fluorescence. For panel E, the filled circles represent individual muscle fibres from a single *mdx* muscle injected with AAV-MuSK-GFP. Arbitrary pixel intensity values are shown on both axes. The open circle shows the mean intensity of utrophin immunofluorescence in the sarcolemma of fibres from the contralateral, empty-vector control muscle. The least-squares line of best fit is shown. **(F)** Muscle proteins were resolved and probed for utrophin using the Wes™ automated capillary electrophoresis system. Three out of four *mdx* muscles that had been injected with AAV-MuSK (mdx + MuSK) revealed a band near the predicted molecular mass of utrophin (392kDa; arrow). Scans of the fourth *mdx* + MuSK capillary, the contralateral empty vector control capillaries (*mdx* empty) and three wild-type muscle samples detected no peaks in the expected range. The capillary/lane labelled C was loaded with sample *mdx* + MuSK 1 and probed with secondary antibody alone (no primary antibody control). The contrast of tone panels was adjusted to facilitate reproduction.

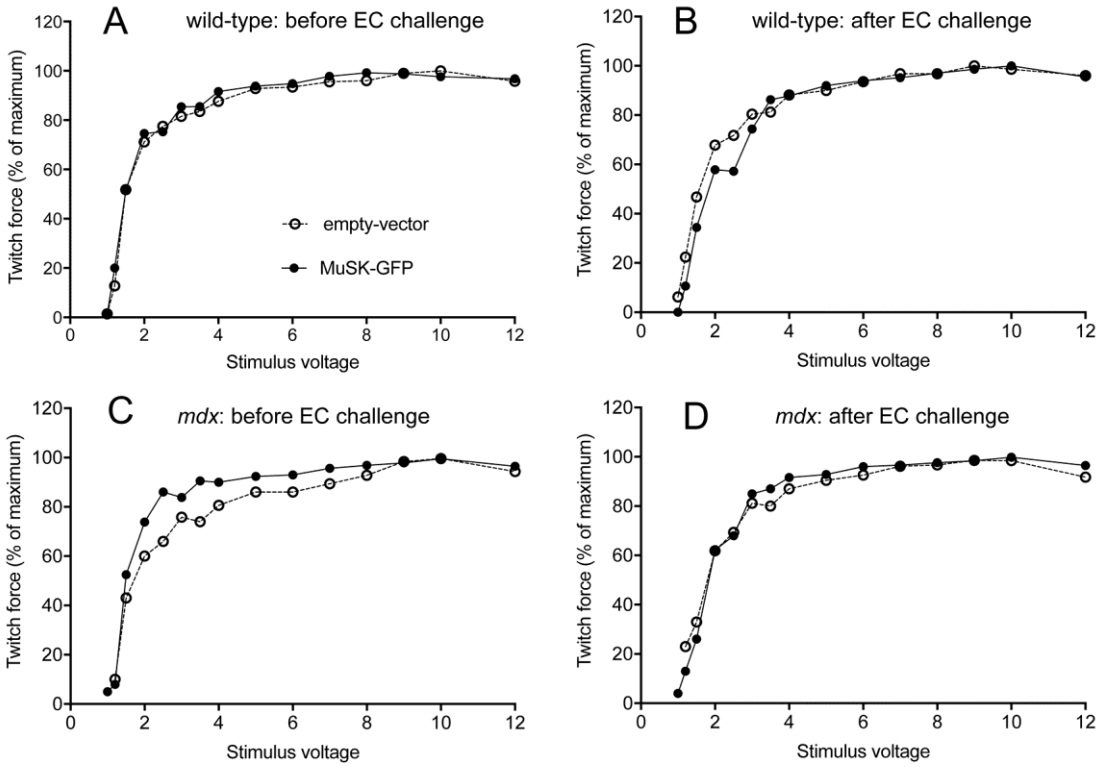

Fig 9 Relationship between twitch-force and the stimulus voltage (applied directly to the muscle). Results are the average for 5-7 muscles before and after they were challenged with a series of 12 nerve-evoked ECs. For each muscle, peak force was normalized to the plateau force value (100%). For clarity only mean values are shown. **(A & B)** Results for wild-type mice before (A) and after (B) the EC challenge. **(C & D)** Results for *mdx* mice before (C) and after (D) EC challenge. Filled circles represent muscles expressing MuSK-GFP, while open circles represent muscles injected with empty AAV vector.

Table 1 Neuromuscular junction properties

NMJ properties Mean (SD) / n muscles	Geno-type	Empty vector		MuSK-GFP		Rapsyn-GFP	
		Not stretched	Stretched	Not stretched	Stretched	Not stretched	Stretched
Endplate AChR area (μm^2)	wt	294 (28) /5	359 (52) /6	289 (88) /3	320 (39) /3	340 (47) /3	362 (43) /3
	mdx	401 (38) /6	395 (28) /7	286 (54) /3	272 (17) /3	348 (40) /3	341 (64) /4
Nerve terminal area (μm^2)	wt	221 (78) /5	287 (46) /6	241 (43) /3	249 (39) /3	226 (69) /3	286 (62) /3
	mdx	309 (19) /6	322 (44) /7	221 (43) /3	237 (8) /3	272 (28) /3	288 (41) /4
Number of AChR patches per endplate	wt	2.9 (0.7) /5	3.5 (1.2) /6	4.1 (1.0) /3	2.3 (1.1) /3	3.3 (0.8) /3	3.7 (1.8) /3
	mdx	6.7 (1.0) /6	7.6 (1.4) /6	8.5 (3.3) /3	6.9 (0.6) /3	5.6 (0.4) /3	8.1 (1.1) /4
AChR density (%)*	wt	100 (14) /4	nd	96 (20) /4	nd	nd	nd
	mdx	87 (17) /6	nd	53 (14) /7	nd	nd	nd
β-dystroglycan density (%)*	*mdx*	108 (34) /5	nd	103 (26) /6	nd	nd	nd
α-syntrophin density (%)*	*mdx*	99 (14) /4	nd	72 (7) /4	nd	nd	nd

nd -not determined

* -intensity of fluorescent labelling of the endplate expressed as a percentage of the mean for wild-type control muscles.